Impacts of climate change on nutrient losses from the Pike River watershed of southern Québec

C. Gombault[1], C. A. Madramootoo[2], A. R. Michaud[3], I. Beaudin[3],
M. F. Sottile[4], M. Chikhaoui[5], and F. F. Ngwa[6]

[1]Department of Bioresource Engineering, McGill University, Macdonald Stewart Building, 21111 Lakeshore Road,
Ste. Anne de Bellevue, Québec, Canada H9X 3V9 (e-mail: colline.gombault@mail.mcgill.ca);
[2]Faculty of Agriculture and Environmental Science, McGill University, Macdonald Stewart Building,
21111 Lakeshore Road, Ste. Anne de Bellevue, Québec, Canada H9X 3V9; [3]Institut de Recherche et
Développement en Agroenvironnement Inc. (IRDA), 2700, Rue Einstein, Québec, Canada G1P 3W8; [4]Ouranos
Consortium 550, Sherbrooke Ouest, Tour Ouest, 19e étage, Montréal, Québec, Canada H3A 1B9; [5]Department of
Natural Resources & Environment, Institut Agronomique & Vétérinaire Hassan II, Rabat,
Morocco; and [6]Brace Centre for Water Resources Management, Stewart Park Three, 21111 Lakeshore Road, Ste.
Anne de Bellevue, Québec, Canada H9X 3V9.

Gombault, C., Madramootoo, C. A., Michaud, A. R., Beaudin, I., Sottile, M. F., Chikhaoui, M. and Ngwa, F. F. 2015.
Impacts of climate change on nutrient losses from the Pike River watershed of southern Québec. Can. J. Soil Sci. **95**: 337–358.
The impacts of climate change on water quality in the Pike River watershed, an important contributor of nutrient loads
into the northern arm of Lake Champlain, were simulated for the time horizon 2041–2070. Four water quality scenarios
were simulated using a calibrated version of the Soil and Water Assessment Tool (SWAT) customized to Québec
agroclimatic conditions. Three of the scenarios were generated using climate data simulated with the Fourth-generation
Canadian Regional Climate Model (CRCM4). The fourth scenario was generated using the climate simulated with the
Arpege Regional Climate Model. Potential mean climate-induced changes in sediment, phosphorus, and nitrogen yield
projected by these scenarios were then analyzed for the 2050 horizon. In addition, the impacts of the different sources of
climate projection uncertainty were assessed by comparing climate model initial conditions, and climate model physical
structure effects on the hydrochemical projections. Only one climate scenario projected a significant increase in mean
annual total phosphorus [10 metrics tons (t) yr^{-1} or 14%] and total nitrogen (260 t yr^{-1} or 17%) loads. However, when
shorter time spans (seasonal and monthly scales) were considered, several significant changes were detected, especially in
winter. Sediment and nutrient loadings, in winter, were predicted to become three to four times higher than current levels.
These increases were attributed to a greater vulnerability of soils to erosion in winter due to the decrease in the snowpack,
early onset of spring snowmelt, a greater number of rainfall events, and snowmelt episodes caused by higher winter and
spring temperatures.

Key words: Water quality modelling, climate change, Soil and Water Assessment Tool, non-point source pollution,
Missisquoi Bay, Lake Champlain, regional climate models

Gombault, C., Madramootoo, C. A., Michaud, A. R., Beaudin, I., Sottile, M. F., Chikhaoui, M. et Ngwa, F. F. 2015.
**Impact des changements climatiques sur la perte de nutriments dans bassin de la rivière Aux Brochets dans le sud du
Québec**. Can. J. Soil Sci. **95**: 337–358. L'impact des changements climatiques sur la qualité de l'eau du bassin versant de la
rivière Aux Brochets, un important contributeur des apports en nutriments du Lac Champlain, a été simulé pour la période
2041–2070. Quatre scénarios de qualité de l'eau ont été simulés à partir d'une version modifiée et calibrée du Soil and
Water Assessment Tool (SWAT). Trois scénarios furent générés à partir de trois climats provenant de la 4ième version du
Modèle Régional de Climat Canadien (MRCC4). Le quatrième scénario fut généré avec un climat simulé par le modèle
Arpège. Les changements moyens de qualité de l'eau projetés par ces scénarios furent analysés pour les exports en
sédiment, phosphore et azote. De plus, l'impact de différentes sources d'incertitudes reliées aux modèles du climat fut
évalué en comparant l'effet des conditions initiales et de la structure physique des modèles climatiques sur les projections
hydro-chimiques. Seul un scénario a projeté une augmentation annuelle significative pour le phosphore total (10 t an^{-1} ou
14%) et l'azote total (260 t an^{-1} ou 17%). Cependant, lorsque l'on considère des pas de temps saisonniers ou mensuels,

Abbreviations: BMP, best management practice; **CP**, coefficient of performance; **GHGe**, greenhouse gas emission; **HRU**, hydrological response unit; **NPS**, non-point source; **NSE**, Nash–Sutclifffe Efficiency; **PBIAS**, percent bias; **SRES**, Special Report on Emissions Scenarios; **SWAT**, Soil and Water Assessment Tool; **TN**, total nitrogen; **TP**, total phosphorus

plusieurs autres changements significatifs, particulièrement en hiver, ont été détectés. Les apports hivernaux en sédiments et nutriments simulés pour 2041–2070 ont triplé voire quadruplé par rapport aux niveaux historiques. Ceci est expliqué par l'accroissement de la vulnérabilité des sols à l'érosion en hiver causé par une diminution de la couverture de neige, l'avancement de la fonte des neiges et un plus grand nombre d'épisodes de pluie et de fonte de neige causés par de plus hautes températures en hiver et au printemps.

Mots clés: Modélisation de la qualité de l'eau, changement climatique, SWAT, pollution agricole diffuse, Baie Missisquoi, Lac Champlain, modèle régional de climat

The Missisquoi Bay, located on the northernmost section of Lake Champlain, is the source of drinking water for several towns (such as Bedford and Phillipsburg in Québec) and supports important economic and recreational activities (aquatic sports, fisheries, resort). The bay and its watershed constitute an exceptional aquatic ecosystem as it provides habitat and spawning grounds for several flora and fauna, amongst which are 25 endangered or threaten species (Union Québecoise pour la Conservation de la nature 2005). However, like many other fresh water bodies surrounded by intensive anthropogenic activities, the bay has suffered from eutrophication attributed to nutrients, particularly nitrogen (N) and phosphorus (P) overloading for almost two decades. These increased nutrient loads have been associated with the dramatic increase in toxic cyanobacteria (blue–green algae) proliferation in the Missisquoi Bay over the past decade [Ministère du Développement durable, de l'Environnement et des Parcs (MDDEP) 2012]. Contamination of these water resources by toxic cyanobacteria poses health risks to lakeshore communities as well as economic impacts that may ensue from decreased tourism (Fortin et al. 2010).

Given this situation, the governments of Vermont and Québec, who share jurisdiction over the Missisquoi Bay and its surrounding watersheds, have committed to reducing P loading, a key driver of cyanobacteria growth (Blais 2002), and eutrophication of lakes (Sharpley et al. 2003).

About 70 to 80% of P loads into the Bay are attributed to non-point source (NPS) pollution from agricultural activities (Hegman et al. 1999; Lake Champlain Basin Program 2012). Despite efforts at reducing NPS pollution, there have been no noticeable reductions in P concentrations in the bay to date (Beck et al. 2012). The bay's P loading capacity of 97.2 t P yr^{-1} has consistently been exceeded since 2001, with average annual loadings approaching 200 t P yr^{-1} (Beck et al. 2012). The Pike River, one of the three main rivers draining into the Bay, discharged an estimated 44 t total P (TP) yr^{-1} into the bay between 2000 and 2003 (Deslandes et al. 2007).

Many studies have investigated NPS pollution issues within the Pike River watershed. Michaud et al. (2002) and Jamieson (2003), for example, reported that P loss from agricultural fields in the Pike River watershed mostly occurred through surface runoff during the snowmelt season or during high-intensity rainfalls. Particulate P

bonded to sediments is typically the dominant form of P (70%) exported out of fields.

Gollamudi et al. (2007) and Eastmann et al. (2010) measured sediment and nutrient exports from agricultural fields with different soil, drainage and fertilization characteristics. They observed substantial loss of sediment and particulate P (1.8 kg ha^{-1} for TP) from clayey soil sites through subsurface runoff, which they attributed to preferential flow. Michaud et al. (2008) showed through diverse simulations using a modified version of the Soil and Water Assessment Tool (SWAT) that considerable reductions in erosion, P, and N export were readily attainable when Best Management Practices (BMPs) were applied to the most erosion-prone areas.

Although implementation of various BMPs can potentially lead to reductions in erosion as well as TP and TN export towards water courses, changes in temperature, precipitation, and extreme events might make current BMPs untenable under future climate. Indeed, climate alterations over southern Québec are expected to accentuate the erosive power of rainfall and runoff and, consequently, to increase the export of sediments and nutrients [Soil and Water Conservation Society (SWCS) 2003; Lettenmaier et al. 2008; Ouranos 2010].

Several studies have looked at the implications of hydrological changes on erosion and NPS nutrient pollution in Québec (Dayyani et al. 2012) and other regions with similar climate conditions (Bouraoui et al. 2002; Arheimer et al. 2005; Booty et al. 2005; Jeppensen et al. 2009; Pierson et al. 2010; Crossman et al. 2013). Some of these studies used climate data from the Regional Climate Model or Global Climate Model to drive physically based impact models such as SWAT (Bouraoui et al. 2002; Rahman et al. 2010), HBV with INCA-P (Crossman et al. 2013), AGNPS (Booty et al. 2005), and CATHY (Sulis et al. 2011). The climate data utilized are typically downscaled with sophisticated statistical methods and/or monthly mean changes (deltas) calculated between two periods of simulated data (future vs. control) and applied on daily observed precipitation and temperatures. Arheimer et al. (2005) investigated the impacts of climate change on N load in southern Sweden and observed seasonal trends with increased runoff and nutrient losses in winter and earlier spring, but a decrease from summer to fall. Similarly, projections by Pierson et al. (2010) showed minimal differences in annual TP loads but significant changes in TP delivery timing due to

greater runoff during winter and a shift of snowmelt earlier in the year in Sweden and Finland.

Crossman et al. (2013) assessed changes in hydrological regime and water quality of the Black River in southern Ontario using a combination of the HBV and INCA-P models driven by statistically downscaled temperature and precipitation projections from the Canadian Coupled Global Climate Model 3 (CGCM3) for two greenhouse gas emission (GHGe) scenarios for the period 2001–2100. Results from this study showed greater winter flows and earlier snowmelt by the end of the century attributable to an increase in rainfall and temperature during winter. Furthermore, the flow regime of the river changed from a snowmelt to a rain-fed regime by the 2090s. Both GHGe scenarios projected increases in annual TP loadings despite the implementation of intensive BMPs within the simulations.

It is therefore obvious from previous studies that climate change could potentially lead to delivery of nutrients into water bodies earlier in the year as a result of earlier snowmelt and increased runoff. To assess climate change impacts and their associated uncertainties it is common practice to inject within impact models a range of potential temperature and precipitation changes (Boé et al. 2009; Boyer et al. 2010; Crossman et al. 2013). The range should be as wide as possible and integrating several simulations constructed with different models, GHGe and parameterization choices (Frigon et al. 2010). This allows assessing uncertainties rising from climate modelling by providing a range in which future climate impacts are expected to occur. Furthermore different sources of uncertainties are known in climate modelling and affect impact modelling outcome (Fowler et al. 2007; de Elia and Cote 2009; Frigon et al. 2010). Using a range of projections as described above allows us to include and get some understanding of the effect of the different sources of uncertainties on the results. To understand to what extent streamflow was affected by the specific sources of climate uncertainty and from where they stemmed, Jha et al. (2004) compared future streamflow scenarios obtained with SWAT and diverse type of climate models (one GCM and one RCM piloted by this same GCM) and found that the Global Climate Model (vs. the Regional Climate Model) had the greatest influence on the results. Similarly, Frigon et al. (2010) and Jha et al. (2006) found, respectively, that runoff and streamflow were very sensitive to model selection and their parameterization.

This study aims at characterizing the impacts of climate changes on the hydrology and nutrient exports of the Pike River watershed. Specifically, research presented here demonstrates the impacts associated with different sources of future climate uncertainty through analysis of projections from climate models using a range of different initial conditions, and different model physical structures. The land use was maintained static as modelling land use change was outside the scope of the study. The field operation management for the reference

scenario was maintained in future simulations in order to assess the impact of climate change in a business-as-usual context.

We believe the results of this study could enable stakeholders in the Pike River basin to develop strategies to better adapt to climate change impacts. Although the results reported here are not transferable to other watersheds, they may form the basis for analyses in other watersheds considering that, to the best of our knowledge, this is the first or one of the first studies to contemplate such analysis of uncertainties with water quality parameters.

MATERIALS AND METHODS

Description of Study Site

The location of the Pike River watershed in relation to the Missisquoi Bay as well as the different hydrological and weather stations used for the hydrologic and climate modelling are presented in Fig. 1. The town of Bedford, located near the shore of the Pike River and 60 km southeast of Montréal, separates the 630-km^2 Pike River watershed into geophysically distinct upstream (390 km^2) and downstream (240 km^2) portions. Some intensive farming is practiced on the more forested and rugged terrains of the upstream section of the watershed. Slopes are on average 5° steep and elevations range from 50 to 710 m above sea level (Deslandes et al. 2007). The downstream section with flatter topography (0.6°) and fertile soils is more suitable for agriculture. Three-quarters of the downstream section is used for intensive corn, soybean and small cereal production. Intensive animal production is commonly practiced within the municipalities of the Missisquoi and Pike River watersheds with 38 867, 40 357 and, 37 530 animal units in the years 1996, 2001 and 2006 respectively (MDDEP 2007). The watershed has been extensively described in previous studies (Deslandes et al. 2007; Michaud et al. 2007).

SWAT Modelling

A modified version of SWAT 2005 (SWAT$_{qc}$; Michaud et al. 2008), with algorithms customized to improve subsurface, tile drainage flow, and surface runoff predictions in Southern Québec, was used to simulate hydrologic processes and NPS pollution changes in the Pike River basin. SWAT (Arnold et al. 1998) has the ability to simulate the hydrologic response of large, heterogeneous, and agriculturally intensive watersheds, based on sound conceptual and physical foundations (Borah et al. 2002; Borah and Bera 2003; Deslandes et al. 2007) and was used several times within the studied watershed.

Gollamudi et al. (2007) and Eastmann et al. (2010) tested the performance of SWAT2000 at simulating the hydrology, sediments, and nutrient losses from four fields within the Pike River watershed and observed that the model had some difficulties partitioning surface runoff and subsurface flow during high flows, which impeded its ability to achieve high performances in simulating
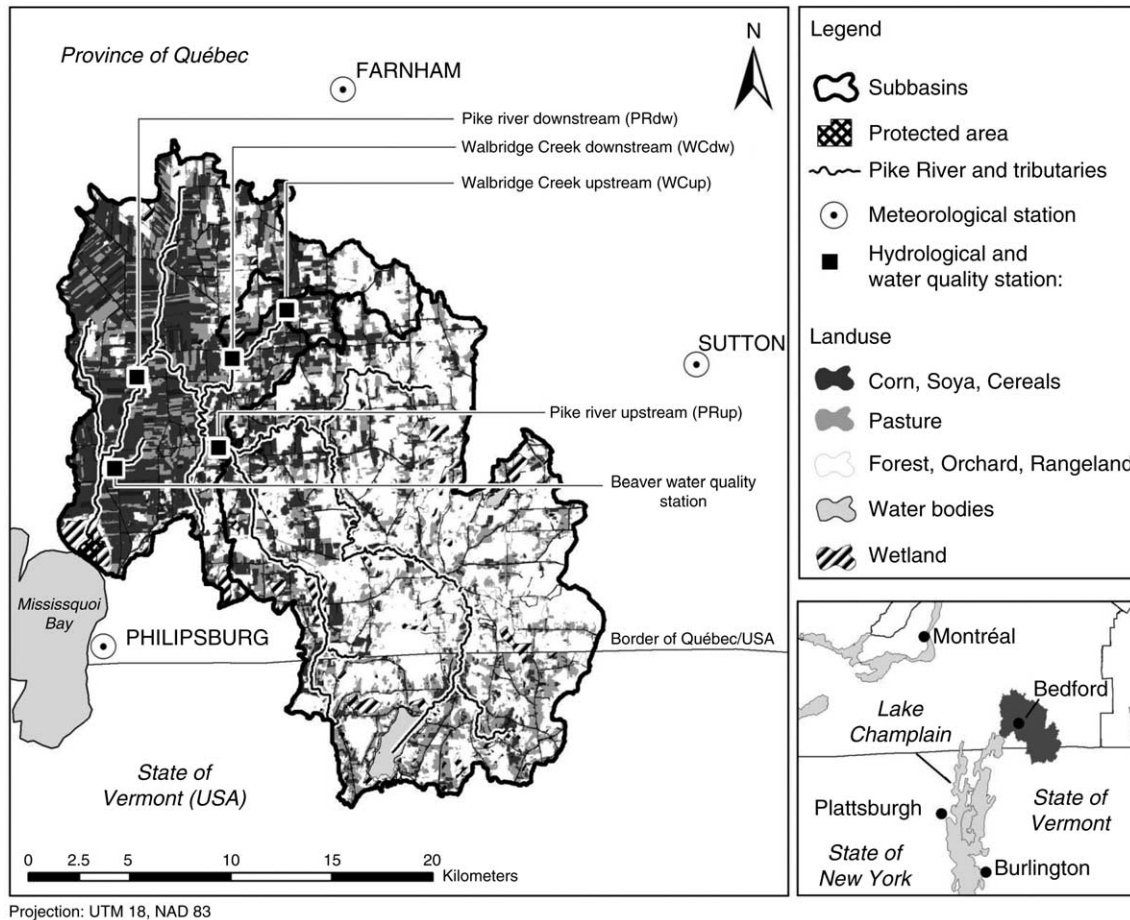
Fig. 1. Maps of the Pike River watershed indicating the location of meteorological and hydrological stations. The land-use data are derived from a Landsat imagery taken in July 1999 (Cattaï 2003).

sediments, particulate P, dissolved P, and TN exports. Nevertheless, they noticed that the model performance remained acceptable especially at annual and seasonal scales.

A similar study by Deslandes et al. (2007) at the watershed scale confirmed the reliability of SWAT2000 at simulating annual and seasonal sediments, TP and NO_3^- loads, despite some difficulties at correctly simulating the magnitude of runoff and streamflow events during winter and spring when temperatures were near $0°C$.

Based on these findings, Michaud et al. (2008) modified the surface retention/runoff ratio in the SCS CN equation in SWAT2005 (the most recent version at the time) from 20:80 to 50:50 to enhance infiltration and diminish surface runoff. The modified SWAT version, called SWATqc, also ensured tile flows were not dependent on water table initialized at 6 m below tiles, but rather on water saturation of the particular soil layers. Last, percolation and preferential flow were directed first to tile flows and then towards the shallow aquifer, contrary to the initial settings. These alterations, after

recalibration, rectified the water balances of intensive agricultural areas as well as nutrient mobilization, especially NO_3^- and soluble P in tile and groundwater. SWATqc therefore offered a better representation of Québec pedo-climatic conditions and as such was deemed a more suitable model for evaluation of the impacts of a combination of BMPs on nutrient losses from agricultural fields (Michaud et al. 2008).

Data for the spatial parameterization of the SWATqc was retrieved from Deslandes et al. (2007) and transferred from SWAT2000 to a SWAT2005 platform (Arnold et al. 1998; http://swatmodel.tamu.edu/contact/). Spatial data (Land use map of July 1999, soils maps, and Digital Elevation Model) entry into SWAT was done through a graphical ArcSWAT interface linked to Arcview 3.3 (ESRI, Redlands CA, http://www.esri.com/). The model delineated 99 sub-basins composed of 1872 hydrological response units (HRU), based on the Digital Elevation Model and overlaying of the soil and the land use map. The HRU is a unique combination of soil, land use, and slope within each sub-basin on which all predictions were based. SWAT allowed soil types with areas accounting

for less than 10% of the sub-basin area to be merged to dominant soil types during the delineation process in order to avoid over-segmentation of the sub-basins.

The initial soil nutrient conditions, for each HRU used in SWATqc parameterization are presented in Table 1. Organic and inorganic fertilizer applications were kept as originally set by Deslandes et al. (2007) and Michaud et al. (2007). The methodology used to parameterize individual HRUs' nutrient inputs and crop uptakes has been initially developed by Deslandes et al. (2004) based on annual expenditures of inorganic fertilizer, livestock composition (for manure), and crop types listed on the government's farm registration record of 2001 at the Québec Ministry of Agriculture, Fisheries, and Food. The dates of field operations were estimated annually for each crop based on annual reports of the State of the Crops from La Financière agricole (2008) and temporal distribution of rainfall events. As such, field operation managements were the same throughout all simulations but their schedule differed among years following rainfall patterns during the calibration and validation period.

Due to the upgrade from SWAT2000 to SWAT$_{qc}$, the model was recalibrated and validated for hydrology, sediment, TP, and NO$_3$- loads using observed daily precipitation and temperatures. The observed climate data were downloaded from the National Climate Archives Database (Environment Canada 2007) for the three stations (Farnham, Sutton, and Phillipsburg) that were closest to the watershed (Fig. 1).

The model was first calibrated to accurately simulate annual evapotranspiration, surface runoff, tile flow, and groundwater flow processes followed by calibration of daily and monthly streamflow against data available from two gauges located upstream (PRup) and downstream (PRdw) (Fig. 1) of the Pike River. This calibration period was from November 2001 to May 2003. Sediment and nutrient data were not available for the main channel of the Pike River, so calibration was performed on "Walbridge Creek upstream" (WCup) and "Walbridge Creek downstream" (WCdw) tributaries and their sub-basin (Fig. 1) for which robust hydrological and nutrient loads were available (Michaud et al. 2004a). Michaud et al. (2004a) estimated daily loadings in sediments, TP, and TN with concentration–discharge rating curves established for three streamflow ranges using Flux 5.0 (Walker 1998). These same loads were used to calibrate SWAT first model of the Pike River by Deslandes et al. (2007), who explained that "The coefficients of variation of load estimates remained within acceptable limits for the modelling of small tributaries (Walker 1998). An inspection of regression residuals for concentration–discharge and load–discharge relationships demonstrated the independence of residuals with respect to discharge, date, season, concentration and load. No outliers were detected (5% confidence level)." More details are provided in Michaud et al. (2004a, b).

The WCup and WCdw tributaries were also calibrated from November 2001 to May 2003. These tributaries and their sub-basins were chosen in previous studies (Deslandes et al. 2007; Michaud et al. 2008) because their specific properties were representative of the upstream and downstream portions of the Pike River watershed. The hydrology of these two sub-basins was calibrated with parameters slightly different from the Pike River watershed to account for their smaller size. Validations of simulated streamflow, sediment, and nutrient exports were performed on distinct periods (Table 2). Streamflows for the Walbridge and the Pike River were obtained from the Centre d'Expertise Hydrique du Québec (MDDEP 2008).

Once the streamflow and nutrient loads were adequately simulated at the WCup and WCdw stations for

Table 1. Initial labile N and P level inputs in SWAT. Nitrate (NO3) default values in SWAT are calculated according to soil depth. Soil depths of first layers vary between 50 mm and 1000 mm but most of the basin soils have depth around 150 to 300 mm

Parameter	Value	Sources
Initial labile N (mg N kg^{-1} soil)	Soil depth (mm): 50:6.65 mg N kg^{-1} 150:6.02 mg N kg^{-1} 200:5.73 mg N kg^{-1} 500:4.24 mg N kg^{-1} 1000:2.57 mg N kg^{-1}	Neitsch et al. (2005, p. 178)
Initial labile P (mg P kg^{-1} soil) Values in the given ranges varies per sub-basin and soil depending on their P richness	Corn: between 31 and 63 mg P kg^{-1} Soybean: between 15 and 31 mg P kg^{-1} Cereals: between 15 and 31 mg P kg^{-1} Hay: between 15 and 31 mg P kg^{-1}	Deslandes et al. (2006)
Mineral and Organic fertilizer application (kg P (or N) ha^{-1} yr^{-1}) Each HRU had a different application rate. Values presented in this table are area weighted averages of yearly application	Corn: 68 P ha^{-1} yr^{-1} and 128 kg N ha^{-1} yr^{-1} Soybean: no fertilizer application Cereals: 112 kg P ha^{-1} yr^{-1} and 51 kg N ha^{-1} yr^{-1} Hay: 61 kg P ha^{-1} yr^{-1} and 117 kg N ha^{-1} yr^{-1}	Québec Ministry of Agriculture, Fisheries, and Food (2000)

Corn area in the watershed was 124 km^2; soybean: 60 km^2; cereals: 44 km^2; and pasture: 138 km^2. The whole watershed area is 630 km^2.

Table 2. Data and periods for the calibration and validation of SWATqc

Station ID	Sub-basin	Drained area at stations (km^2)	Calibration period	Validation period	Available data	Basin description	Sources of the data
PRup	Pike River upstream from Bedford	390	Nov. 2001– May 2003	Jun. 2003– Dec. 2011 and Nov. 1979– Dec. 2000	Daily streamflow – Ice effect leads to streamflow overestimation during winter	Rolling landscape, mainly wooded	CEHQ
PRdw	Pike River down-stream from Bedford	561	Nov. 2001– May 2003	Jun. 2003– Dec. 2011	Daily streamflow – Ice effect	Drains the rolling and forested lands of the water-shed's headwaters and a portion of the flat, agricul-tural lands	CEHQ
WCup	Upstream Walbridge Creek	6.3	Nov. 2001– May 2003	May 2004– Sep. 2006	Daily streamflow – Ice effect corrected	Rolling and agricultural (61%), typical landscape of the Appalachian piedmont	Streamflow: CEHQ Water quality: Michaud et al. (2004a)
WCdw	Downstream Walbridge Creek	7.9	Nov. 2001– May 2003	May 2004– Sep. 2006 (streamflow) Nov. 2001– May 2006 (nutrient loads)	Daily streamflow Monthly sediments, total P and total N loads – Ice effect corrected	Flat and agricultural (63%), long slopes, typical of St. Lawrence lowlands	Streamflow: CEHQ Nutrient loads: Michaud et al. (2004a)
Beaver	Beaver Creek, located within the downstream portion of the watershed	11	No calibration	Jan. 2001– Aug. 2011 (streamflow) Jan. 1998– Mar. 2003 (nutrient loads)	Daily streamflow, monthly sediments, total P loads	Flat and agricultural (97%), long slopes, typical of St. Lawrence lowlands	Streamflow: CEHQ Nutrient loads: Michaud et al. (2004b)

The periods of calibration and validation were determined based on the availability and robustness of the data.

the calibration and validation periods, the calibrated nutrient load parameters for each of the Walbridge sub-basins were transferred to the respective upstream and downstream sections of the Pike River watershed. To verify the adequacy of transferred nutrient load parameters from the experimental sub-basins to the whole basin, a third sub-basin of the Pike River–Beaver sub-basin for which reliable data were available (Michaud et al. 2004b) was used. Table 2 summarizes the data and the periods used to calibrate and validate the model during the present study.

Runoff was estimated by the SCS Curve Number method (US Departement of Agriculture–Soil Conservation Service 1972), evapotranspiration by the Hargreaves method (Hargreaves et al. 1985), and the routing of flow through the hydrological network by the Muskingum method (Overton 1966). Sediment load estimation in the model was performed using the Modified USLE equation (Williams 1975), whereas P and N loads were estimated with a loading function (Williams and Hann 1976).

In summary, the calibration was performed in accordance with the established method as described in Moriasi et al. (2007) and Arnold et al. (2012). The method used was a process-based calibration. The annual water balance was calibrated for all main and important hydrological processes (runoff, infiltration, percolation, subsurface flow) as well as for streamflow at daily, monthly and annual time steps. To ensure that hydrological processes were well reproduced, the calibration and validation were performed on different sub-basins with different physical characteristics (PRup, PRdw, WCup, WBdw). The upstream section was first calibrated and validated before the downstream section of the Pike River watershed. The detailed results of the hydrological calibration are presented in Gombault et al. (2015). Sediment load was first calibrated followed by TP and then TN loads to ensure adequate reproduction of physical processes and consequently better modelling of related processes (Arnold et al. 2012). The area used to calculate the watershed nutrient exports by the Pike River is the area of the whole Pike River watershed, 630 km^2.

Model performance was assessed using the three recommended coefficients of performance (CP), coefficient of determination (R^2), Nash–Sutcliffe Efficiency (NSE) and percent bias (PBIAS), described in Moriasi et al. (2007). R^2 and NSE values of 1 and PBIAS of 0 represent a perfect fit between simulated and measured data. Although NSE values between 0 and 1 are generally acceptable, modellers usually aim for a minimum value of 0.5.

Climate Change Projections
Climate impact assessments are conventionally performed using a large number of climate model projections (all plausible and equally likely to occur) in order to encompass as many sources of uncertainty as possible.

This approach is, however, time consuming and requires large computational resources. To circumvent these constraints, only four climate projections were used in this study. The four projections were purposely chosen to account for a wide range of plausible changes in future climate while also encompassing the possible uncertainties arising from modelling techniques. The four projections were produced by the Ouranos Consortium, a leader in climate change modelling in Canada. The four projections consisted of paired climate datasets simulated on historical (1971–2000) and future (2041–2070) periods and are named ADC, ACU, AFA/AFD and ARP. The characteristics of these four projections used in this study are presented in Table 3.

Three projections, ADC, ACU, and AFA/AFD, came from the CRCM4 (versions 4.1.1 and 4.3.2) (Caya and Laprise 1999; Plummer et al. 2006) which was driven by CGCM3 version 3.7.1 (Scinocca and McFarlane 2004; McFarlane et al. 2005) using different initial conditions (start day simulations) for each projection. In addition, the domain of the CRCM4 version 4.1.1 was centred on Québec, while version 4.3.2 covered the larger North American (AMNO) domain. The fourth and final projection, ARP, came from a completely different model, the French model, using variable grid Arpège version 4.4, member 1 (Douville et al. 2002; Gibelin and Déqué 2003). The grid points of the RCM were chosen so that their centres fell as close as possible to the meteorological stations used to calibrate SWAT. Although the spatial resolution of the pilot CGCM3 was 200 km × 200 km, the final dataset had a 45 km × 45 km resolution akin to the CRCM4 or Arpège models. The GHGe scenario A2, representative of a regionally oriented, fragmented, and slower economic growth (Nakicenovic et al. 2000), was integrated in the four future (2041–2070) climate simulations, while radiative forcing corresponding to pre-industrial to the 2000 GHGe historical records were utilized for the historical (1971–2000) simulations. Other scenarios from the Special Report on Emissions Scenarios (SRES), such as B1 or A1B, etc., presented only minor differences in the global surface warming for the time horizon chosen in this study [Fig. 10.4, Working Group I report of the Intergovernmental Panel on Climate Change (IPCC) 2007]. Hence it was assumed that inclusion of all SRES scenarios would not result in significant improvements in the capture of uncertainties. The fact that A2 is one of the GHGe scenarios projecting the highest increase in greenhouse gas emission let us to believe that use of this scenario should permit development of robust Watershed Management Plans to withstand future climate-induced impacts. Recent studies showed that concentrations of GHGe recorded between 2000 and 2005 already exceeded A2 projections for this period (Raupach et al. 2007).

The CGCM3 and CRCM4 were among the latest and most widely assessed models (Plummer et al. 2006; Frigon et al. 2010; Music 2011) available at the beginning of our study. Furthermore, both models have been thoroughly compared with other models prior to use in

Table 3. Characteristics of the climate datasets driving SWATqc

Name of the climate simulations	Time window	Regional climate model (RCM)	Driver of the RCMs	GCM member (expressing initial conditions)	RCM domain (cells × cells)	GHG emissions scenario
ACZ	1971–2000	CRCM 4.1.1	Reanalysis ERA40	None since driven with reanalysis	Québec (112 × 88)	Historical measurements
ADC	1971–2000 and 2041–2070	CRCM 4.1.1	CGCM3 3.7.1	1	Québec (112 × 88)	SRES A2
ACU	1971–2000 and 2041–2070	CRCM 4.1.1	CGCM3 3.7.1	4	Québec (112 × 88)	SRES A2
AFA/AFD	1971–2000 and 2041–2070	CRCM 4.2.3	CGCM3 3.7.1	5	AMNO (182 × 174)	SRES A2
ARP	1971–2000 and 2041–2070	Arpège 4.4	No driver Arpège Variable grid mesh	1	T 159 (182 × 174)	SRES A2

the production of sound physically based climate simulations (NARCCAP 2007; Music 2011) as part of an international global assessment over North America. The Arpège model has been successfully used to predict climate change impacts in snowmelt and rainfall watersheds (Boé et al. 2009). The availability of Arpege data from the Ouranos Consortium provided us with an opportunity to use this model to assess a wider range of possible future climate change impacts. Furthermore, the use of Arpège in conjunction with CRCM4 enabled us to evaluate uncertainties that may arise from differences in the conceptualization of the models' physical processes. Figure 2 shows how CGCM3 and the four chosen regional projections compare with 130 projections from an ensemble of other global climate models (including the renowned CSIRO, ECHAM, and HadCM3 models). Generally, CGCM3 projections fall within the wetter part of the ensemble, with 11 projections out of 14 showing annual average precipitation increase above 5% of the current level (about half of all projections are either above or below this 5%). The model also projects a warm future, but remains within the centre of the ensemble with 14 of its projections showing annual average temperature increase between 1.3 and 3°C. The five projections from CSIRO, by contrast, are located in the wet part of the ensemble, but remain within the first 50% of the ensemble with temperature increases below 2.5°C. ECHAM tends to be as wet and warm as CGCM3 with nine projections falling within 50% of the wetter projections. Only one projection of ECHAM is in the wet and colder part of the ensemble. Finally, HadCM3 with only four projections sits in the hot and dry part of the ensemble with three projections having precipitation increase below 5% and temperature increase between 2 and 4°C. Figure 2b shows that the four projections regionally downscaled with CRCM4 cover as wide a spectrum of uncertainty as could have been achieved by using a range of GCMs.

ADC, ACU, AFD/AFA, and ARP projections were chosen to cover as wide a range of plausible scenarios as possible whilst incorporating small-scale variation (and
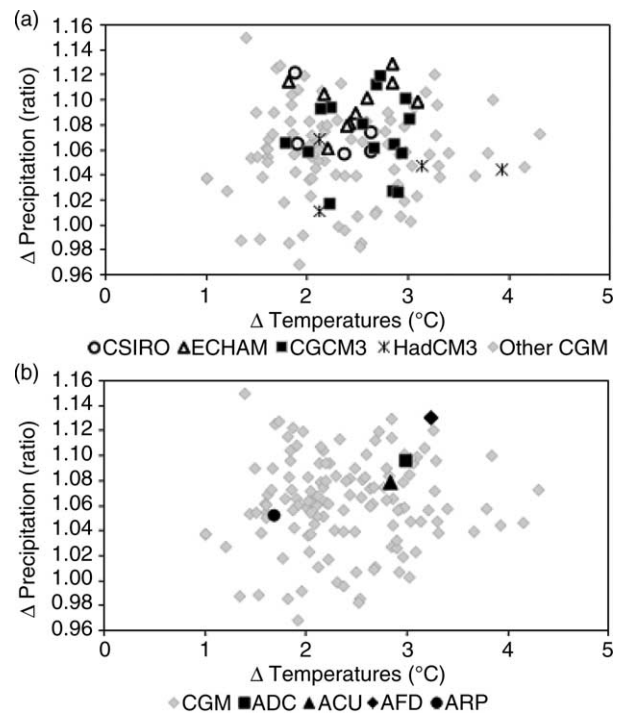

Fig. 2. Annual average changes in temperatures and precipitation in Missisquoi Bay watershed between 1971–2000 and 2041–2070 as projected by 130 simulations run with three Special Report on Emissions Scenarios GreenHouse Gaz emission (SRES GHGe) scenarios A2, B1 and A1B and 16 Global Climate Models (GCM) including (a) the internationally used CSIRO, ECHAM, CGCM3 and HadCM3 and (b) the four regional projections simulated with CRCM4 and used in this study.

associated impacts) within that range (Fig. 2). For example, the ADC and ACU projections were chosen because they were in the wet and warm part of the ensemble and only differed in their initial conditions (member only), thus making the two projections more similar relative to ARP or AFD/AFA. This allowed for the assessment of small-scale impact variations. The ARP projection was chosen not only because it was drier and cooler than the three other projections simulated by CGCM3, but also because it came from a model with a structure completely different from CGCM3 or CRCM4. This allowed us to assess and quantify uncertainty arising from the use of different models. The AFD/AFA was chosen because it allowed us to incorporate a projection with a wetter and hotter climate, thus allowing us to assess and quantify uncertainty arising from the use of different versions and domains of the CRCM4.

Although the four climate projections were dynamically downscaled from the GCMs with CRCM4 or the Arpège variable resolution grid, it is known that CRCM4 monthly mean outputs may still differ from local records (Gagnon et al. 2009). Although these biases do not invalidate the projected changes, they nevertheless signal uncertainties due, for instance, to internal model variability (de Elia and Coté 2010) or scaling issues causing discrepancies between the climate recorded at a station and the climate simulated for a 45-km × 45-km grid area (model grid resolution). Figure 3 shows these biases for our four projections over the Pike River basin. The CRCM4 typically underestimates historical winter and summer precipitation by up 40% and 75%, respectively. Temperatures are typically underestimated all year round between about 1 and 3.5°C by most projections and up to 5°C by AFA. Greater underestimations of temperature were witnessed in winter and spring when accuracy of this variable is particularly important given its influence on snowfall and snowmelt and, consequently, on runoff. Contrary to CRCM4 simulations, the Arpège simulation overestimates winter temperature and precipitation.

The perturbation (aka delta change) method or other complex statistical methods are amongst the approaches commonly used to correct bias in climate data. Complex downscaling methods account for changes in precipitation intensity and frequency, but require high statistical expertise and computing resources. The delta change method was used in this study as it allows keeping the proportional differences between the initial simulations, which the statistical method would have altered. Briefly, the ratio of monthly changes in precipitation (or differences, in the case of temperature) between RCM simulations of historical and future values was calculated and applied to the daily observed precipitation and temperature (Eq. 1). A drawback of this method is that it does not account for changes in precipitation frequency and intensity. In order to at least include some changes in precipitation intensity, the maximum half hour rainfall (RAINHMAX) values produced by the RCM for
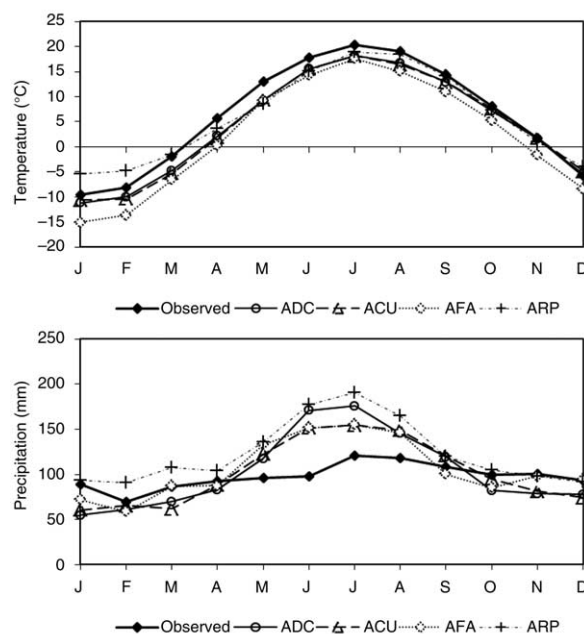

Fig. 3. Comparison of monthly mean temperatures (top) and precipitation (bottom) for the period 1971–2000.

historical and future simulations were used in SWAT simulations. During calibration, RAINHMAX was set with default SWAT values (RAINHMAX 40-yr monthly mean, recorded for Plattsburgh, NY, at about 40 km from the watershed and the closest city in the SWAT database). The same statistics (for 30 yr) were simulated by the regional climate models for the future simulations. The effect of the RAINHMAX parameter on the results of the baseline simulation (with observed climate data) and simulations with the RCM climate data was minor. Therefore, RAINHMAX and the intensity of precipitation are little discussed in this manuscript. Finally, SWAT outputs were compared with a baseline simulation obtained with observed data.

$$Pcp_i = Pcp_{obs} * \frac{\overline{Pcp, m}\,f}{\overline{Pcp, m}\,p}. \tag{1}$$

where Pcp_i is the corrected daily precipitation of the month of year number 1, 2, 3 etc., Pcp_{obs} is the observed daily precipitation of the month of year number 1, 2, 3 etc., $\overline{Pcp, m}\,f$ is the monthly average of precipitation of the month m for the future RCM simulation, and f, $\overline{Pcp, m}\,p$ is the monthly average of precipitation of the month m for the past RCM simulation, p.

Similar equations are applied for minimum and maximum temperature:

$$Tmp_i = T_{obs} * (\overline{Tmp, m}\,f - \overline{Tmp, m}\,p) \tag{2}$$

where Tmp_i is the corrected daily maximum or minimum temperature of the month of year number 1, 2, 3 etc., T_{obs} is the observed daily maximum or minimum temperature

of the month of year number 1, 2, 3 etc., $\overline{Tmp,m}\,f$ is the monthly average of maximum or minimum temperature of the month m for the future RCM simulation, f, and $\overline{Tmp,m}\,p$ is the monthly average of maximum or minimum temperature of the month m for the past RCM simulation, p.

RESULTS AND DISCUSSION

SWAT Performance

For streamflow calibration, CPs for each of the four hydrological stations fell within the "satisfactory" to "very satisfactory" range of Moriasi et al. (2007) as shown in Table 4. In fact, R^2 and NSE values on a monthly basis exceeded 0.7 and 0.5, respectively, while absolute deviation remained below 25%. Although CPs for the validation period were slightly lower, they nevertheless met the recommended performance criteria. SWAT's long-term performance was considered acceptable given that monthly streamflow predictions over the past 20 yr (1980–2000) matched observed data (NSE value of 0.55), and the annual water budget reproduced over the historical period (1971–2000) corresponded to current conditions estimated for the watershed (Table S1). This shows that $SWAT_{qc}$ can reproduce natural variability in streamflow on a long-term basis.

Although limited data were available for the calibration and validation of nutrient loadings, CPs for the calibration period generally met high performance criteria on a monthly basis, while the validation period did not meet CP criteria in a few instances (Table 5). The CPs nevertheless remained within the satisfactory range both for a different period (calibration and validation periods) and for the 3rd sub-basin (Beaver). Total phosphorus loads tended to be low until the GWSOLP parameter was set at 0.07 or 0.08 ppm (Table S2). GWSOLP is a fixed concentration of soluble P in the groundwater contribution to streamflow. Nitrate loads could not be satisfactorily validated due to the lack of data. The CPs presented in this manuscript are lower than those reported by Deslandes et al. (2007), probably because they were computed over longer periods encompassing greater

climate variations. A visual comparison of observed and simulated streamflow, sediment, TP, and N loads for the calibration, validation and evaluation period is shown in Figs. 4, 5, 6, and 7.

SWAT generally tended to overestimate sediment and TP loads mainly in March or April (year 1998, 1999 for the Beaver basin and in 2001, 2003 for Walbridge). Overestimation or underestimation commonly occurred at the beginning of the snowmelt season, when sediment and nutrient losses are at their highest in the region (Jamieson et al. 2003; Deslandes et al. 2007). These imperfections could be attributed to the limitations of SWAT in simulating snowmelt or snowfall at temperatures close to $0^{\circ}C$ as explained in Deslandes et al. (2007). Nonetheless, sediment and TP load predictions mimicked streamflow predictions, with the model adequately reproducing the observed seasonal variability.

The validation periods did not show improvements in model predictions comparable with the calibration period. This is probably because models are often optimized for conditions prevailing during the calibration period, which may differ significantly from the validation period. In this study, the wetter conditions and more intense hydrologic events prevailing during the validation (vs. calibration) period might explain why some CPs were below the recommended value during the validation period (Engel et al. 2007). The weaker validation performance does not invalidate the suitability of the model for simulated processes, but raises awareness of the difficulties associated with simulating sediments and nutrient loads during intense hydrological events and the potential impacts on future projections. Except for the validation of NO_3^-, low NSE values were always above 0 and close to 0.5. Engel et al. (2007) pointed out that the acceptability criteria might be lowered depending on the project objectives.

For the current climate change assessment, we assume that the ability of SWAT to reproduce the principal erosion and nutrient losses processes are acceptable because: (i) CPs indicated that predictions using the calibrated model were significantly improved compared

Table 4. Coefficients of performance for monthly streamflow for the calibration and validation periods

Basins	Period	Number of daily mean observations	NSE	R^2	PBIAS
Recommended CP values on a monthly basis by Moriasi et al. (2007)			*0.50*	*0.50*	*±25.0*
PRup	Calibration: Nov. 2001–May 2003	566	0.69	0.75	13.6
	Validation: Jun. 2003–Dec. 2011[z]	3014	0.52	0.67	20.0
	Evaluation (long-term): Jan. 1980–Dec. 2000		0.55	0.61	14.8
PRdw	Calibration: Nov. 2001–May 2003	566	0.67	0.71	14.1
	Validation: Jun. 2003–Dec. 2011[z]	3014	0.41	0.61	18.1
WCup	Calibration: Nov. 2001–May 2003	566	0.84	0.86	6.6
	Validation: May 2004–Sep. 2006	883	0.51	0.60	−11.7
WCdw	Calibration: Nov. 2001–May 2003	566	0.70	0.74	3.5
	Validation: May 2004–Sep. 2006	883	0.60	0.62	−15.6
Beaver	Validation: Jan. 2001–Apr. 2007	3317	0.50	0.65	23.7
	Jan. 2009–Aug. 2011		0.54	0.41	26.6

[z]For the validation June 2003 to Dec. 2011, winter data of 2008 were discarded. In 2008, the quantity of precipitation and snow attained records.

Table 5. Coefficients of performance for water quality for the calibration and validation periods

Basins	Period	Water quality sample numbers	Sediments			TP loads			NO$_3$ loads		
			NSE	R^2	PBIAS	NSE	R^2	PBIAS	NSE	R^2	PBIAS
Recommended CPs values on a monthly basis by Moriasi et al. (2007)			*0.50*	*0.50*	*±25*	*0.50*	*0.50*	*±25*	*0.50*	*0.50*	*±25*
WCup	Calibration: Nov. 2001–May 2003	166[z]	0.64	0.70	1.85	0.71	0.75	15.60	0.65	0.76	9.98
WCdw	Calibration: Nov. 2001–May 2003	166[z]	0.44	0.59	17.80	0.63	0.68	−0.93	0.50	0.65	23.63
	Validation: Nov. 2004–May 2006	—[y]	0.43	0.46	16.34	0.32	0.35	−8.95	−0.02	0.37	4.00
Beaver	Validation: Jan. 1998–Sep. 2003	150[x]	0.19	0.50	27.70[w]	0.57	0.63	31.5[w]	–	–	–

[z]166 water samples were collected along with continuous (15-min records) monitoring of streamflow between November 2001 and May 2003. Concentration–discharge rating curves established for three streamflow ranges, allowed for the Flux 5.0 (Walker 1998) to estimated daily loadings in sediments, total P and total N. The loads were summed to obtain monthly values. See Michaud et al. (2004a) for detailed explanation.
[y]Michaud et al. (unpublished data). Daily and monthly loads were estimated as in footnote [z].
[x]150 water samples were taken for the period 1999 to 2003 (Michaud et al. 2004b). Daily and monthly loads were estimated as describe in footnote [z].
[w]The recommended range for PBIAS ±25% corresponds to a very good rating. A satisfactory rating is around ±40% depending on the variable (Moriasi et al. 2007).

with those from the un-calibrated model and (ii) the assessment is based on a relative comparison rather than a comparison of absolute values. Calibration parameters are presented in Table S2.

Precipitation and Temperature Changes

Changes in precipitation are ratios of average precipitation between the future and historical periods, while temperature changes are deltas between future and historical monthly mean temperatures (Table 6). For the four projections used in this study, the greatest increases in temperature were typically projected in winter except for ARP, which projected the smaller increase (1.12°C) throughout all projections and seasons. This makes winter the season with the largest range of projected changes (4.18°C) with a mean increase approaching 3.63°C in January. Temperature changes in winter are of particular interest because this is the period when greater impacts are expected in the region (Boyer et al. 2010). The greatest increases in precipitation throughout the four projections also occur in winter or spring with increases approaching 60 and 40% in January and April, respectively. Precipitation projections ranged between −3 and 56% for winter and between 6 and 39% for spring. The narrower range in spring compared with winter suggests less uncertainty. Similarly, there was better agreement between all four projections in summer than in the other seasons. Summer temperatures of the four projections were similar to spring projections although temperature increase were slightly higher in summer reaching monthly mean of 2.95 vs. 2.75°C in spring. Summer precipitations for all four projections showed moderate decreases (3 to 11%), except for projection ARP, which showed an increase of 11%. The increase in fall temperature varied between 1.57 and 3.38°C with a difference of 1.81°C between the lower and higher projections, while precipitation changes varied between −9 and +20%.
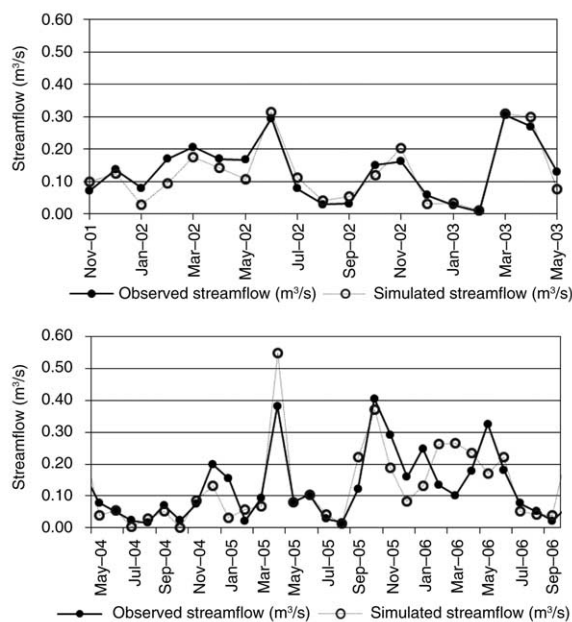

Fig. 4. Observed and simulated streamflow at the outlet of the Walbridge Creek upstream subwatershed during the calibration (top) and validation (bottom) periods.
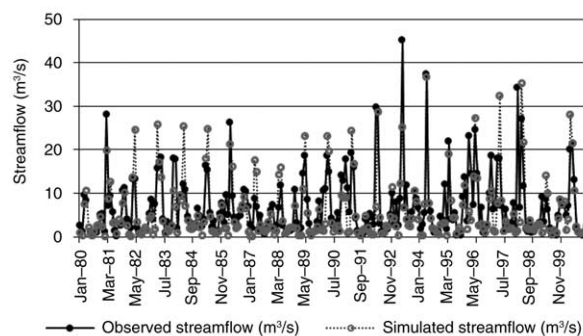

Fig. 5. Comparison of observed and simulated streamflow at PR$_{up}$ station for the evaluation period.
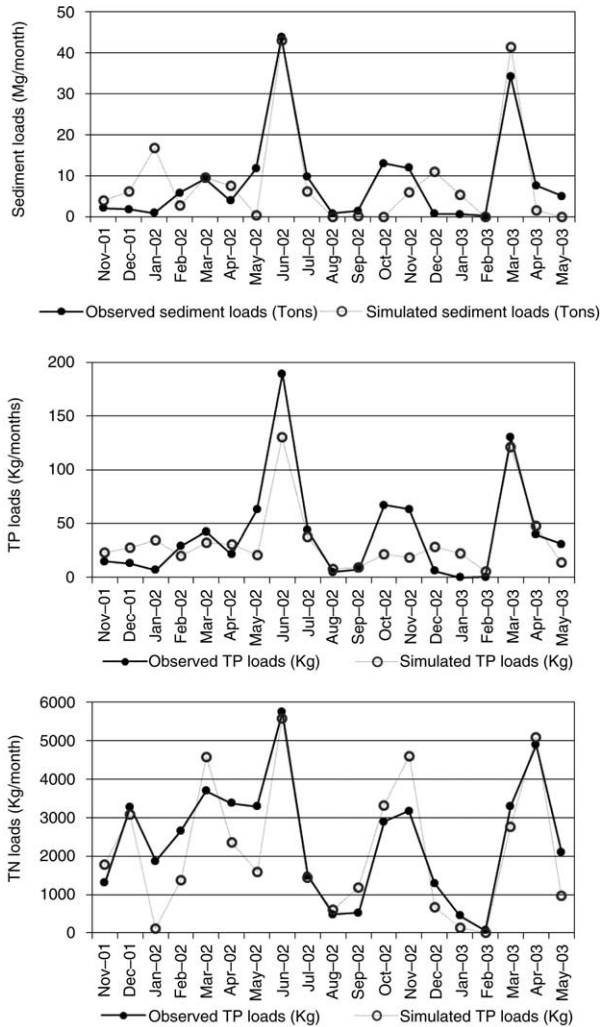
Fig. 6. Observed and simulated sediments and nutrient loads at the outlet of the Walbridge Creek upstream subwatershed for the calibration period. Sediments (top), TP (middle) and TN (bottom).

Fig. 7. Observed and simulated streamflow (top), sediment (middle) and TP (bottom) loads at the outlet of the Beaver Creek subwatershed for the validation period.

For the precipitation, the average of the four projections was generally smaller than the differences between their maximum and minimum changes, which makes the signal of climate change weaker compared with uncertainties (climate change possibilities). The reverse was observed for temperatures, where the mean of the four projections was greater than the difference between the maximum and minimum changes given by the projections, thus making the signal of climate change strong compared with uncertainties. On an annual basis, ADC seems to be the wetter projections (14% increase) and ARP the drier (7% increase). The more extreme changes in precipitation (56% in February and −8 and −9% in summer) were, however, projected by AFA/AFD. AFA/AFD also appeared to be the warmest projections with more extreme increase in temperature (5.36°C in January), while ARP was the coldest. For all seasons, the

Arpège model projected low to moderate changes in temperature and precipitation compared with other GCMs and ensemble members.

Potential Impacts of Climate Change on Water Quality

Mean annual and monthly changes in sediment, TP and TN loading projected for the 2041–2070 period are presented in Tables 7, 8, and 9, respectively. Changes in surface runoff and streamflow are also presented in supplemental material (Tables S3 and S4) to facilitate the interpretation of changes in sediment and nutrient loadings.

Mean annual sediment, TP, and TN exports to the Missisquoi Bay increased from 1 to 7% (70 to 910 t), 13 to 20% (7 to 11 t), and 24 to 43% (372 to 688 t), respectively. The AFD projection, with the greatest increase in winter temperature (4.2°C) and precipitation

Table 6a. Mean monthly precipitation (a) and temperature (b) changes over the Missisquoi Bay as projected by the four chosen regional simulations ADC, ACU, AFD and ARP

Month	Δ ADC	Δ ACU	Δ AFD	Δ ARP	Mean of Δ scenarios	Range of Δs (ΔRange)	Climate change signal If mean >ΔRange signal =strong
	(%)				(%)		
J	26	24	20	14	20	10	Strong
F	28	−3	56	4	20	60	Weak
M	26	35	17	18	20	20	Strong
A	39	19	17	30	30	20	Strong
M	22	13	14	6	10	20	Weak
J	−7	11	5	10	0	20	Weak
J	−4	−9	−8	−3	−10	10	Weak
A	4	−5	−9	−11	−10	10	Weak
S	3	5	6	20	10	20	Weak
O	18	−2	13	−9	10	30	Weak
N	4	2	21	−3	10	20	Weak
D	24	33	15	14	20	20	Strong
Annual Mean	**14**	**11**	**12**	**7**	**10**	**10**	**Strong**

The mean of the four scenarios and the range of changes (ΔRange) for 2041–2070. The comparison of the mean to ΔRange is used to assess the strength of climate change signal of the ensemble mean. Δ % is calculated following this equation: $[(\text{Future } \mu - \text{Baseline } \mu)/\text{Baseline } \mu] \times 100$, where μ is the 30-yr monthly average. ΔRange = ΔMax. − ΔMin.

Table 6b. Mean monthly temperature (b) changes over the Missisquoi Bay as projected by the four chosen regional simulations ADC, ACU, AFD and ARP

Month	Δ ADC	Δ ACU	Δ AFD	Δ ARP	Mean of Δ scenarios	Range of Δs (ΔRange)	Climate change signal If mean >ΔRange signal =strong
	°C				°C		
J	4.23	3.74	5.36	1.19	3.63	4.17	Weak
F	3.99	3.47	3.83	1.12	3.10	2.86	Strong
M	2.55	3.08	2.57	1.28	2.37	1.81	Strong
A	2.77	3.05	2.75	2.03	2.65	1.02	Strong
M	3.43	2.57	2.43	2.56	2.75	1.00	Strong
J	2.20	2.34	3.11	2.38	2.51	0.91	Strong
J	2.80	3.13	3.06	1.98	2.74	1.15	Strong
A	3.16	3.07	3.36	2.19	2.95	1.17	Strong
S	2.71	2.31	2.88	0.95	2.21	1.93	Strong
O	2.54	2.13	2.76	1.77	2.30	0.99	Strong
N	2.17	2.21	3.28	1.57	2.31	1.71	Strong
D	3.27	2.84	3.41	1.17	2.67	2.24	Strong
Annual Mean	**2.98**	**2.83**	**3.23**	**1.68**	**2.68**	**1.55**	**Strong**

The mean of the four scenarios and the range of changes (ΔRange) for 2041–2070. The comparison of the mean to ΔRange is used to assess the strength of climate change signal of the ensemble mean. Δ % is calculated following this equation: $[(\text{Future } \mu - \text{Baseline } \mu)/\text{Baseline } \mu] \times 100$, where μ is the 30-yr monthly average. ΔRange = ΔMax. − ΔMin.

(>30%), projected the greatest increases in TP and TN loads on a yearly basis. The ADC projection with an increase in winter temperature and precipitation of 3.8°C and 16%, respectively, projected an increase in TP loads similar to AFD. In contrast, projection ARP, with smaller temperature and precipitation increases in winter (1.2°C and 6%, respectively) and in the other seasons, projected greater increases in sediment loads and runoff (Table S3).

On a monthly basis, the three CGCM3 climate scenarios (ADC, ACU, and AFD) projected significant increases in surface runoff, sediment, TP, and TN loadings from September to February and until March for TN. A decrease was generally observed from March to August, except for May and June, when small increases were projected. The ARP climate scenario projected slightly different results with increases in all variables witnessed in September and from December to March. The decreases in loadings for the ARP projections in April and on some occasion in summer and fall were similar to the other three projections (Fig. 8).

There was general agreement about the direction of change and significance of results among all four projections except for the ARP projection (obtained with the Arpège model), which showed smaller differences. Generally, greater increases were projected during the

Table 7. Mean annual and monthly total sediment loadings (t) for the baseline (1971–2000) as well as the projected changes (Δ, %) for scenarios ADC, ACU, AFD and ARP, the mean of the four scenarios, and the range of changes (ΔRange, t) for 2041–2070

Month	Baseline observed (t)	ADC Future (t)	Δ ADC (%)	ACU Future (t)	Δ ACU (%)	AFD Future (t)	Δ AFD (%)	ARP Future (t)	Δ ARP (%)	Mean of Δ scenarios (t)	Range of Δs (ΔRange) (t)	Climate Change Signal If mean >ΔRange signal =strong
J	437	2 599	**494**	2 070	**373**	2 217	**407**	799	**83**	1 484	1 799	Weak
F	919	2 837	**209**	2 525	**175**	3 485	**279**	1 312	**43**	1 621	2 173	Weak
M	7 462	5 576	−25	6 957	−7	5 498	−26	8 795	18	−755	3 297	Weak
A	3 819	1 342	**−65**	921	**−76**	1 073	**−72**	2 454	**−36**	−2 371	1 533	Weak
M	21	61	**189**	31	49	31	46	33	**56**	18	30	Weak
J	19	10	**−47**	19	5	14	**−24**	20	7	−3	10	Weak
J	49	21	**−58**	17	**−64**	16	**−67**	28	**−42**	−28	12	Weak
A	38	27	−28	20	−46	12	−69	18	**−52**	−19	16	Weak
S	40	52	**30**	52	29	59	**47**	120	**198**	31	68	Weak
O	198	296	**50**	163	−18	283	**43**	140	**−29**	22	156	Weak
N	298	209	**−30**	420	**41**	362	21	194	**−35**	−2.13	226	Weak
D	496	884	**78**	1 137	**129**	816	**64**	793	60	411	344	Strong
Annual Mean	1 150	1 160	1	1 194	4	1 156	1	1 225	7	34	70	Weak
Annual Sum	13 796	13 914	1	14 334	4	13 866	1	14 706	7	409	839	Weak

The comparison of the mean to ΔRange is used to assess the strength of climate change signal of the ensemble mean. Bold values indicate statistically significant differences between the historical and future periods of study. Δ % is calculated following this equation: [(Future μ − Baseline μ)/Baseline μ] × 100, where μ is the 30-yr monthly average. ΔRange = ΔMax. − ΔMin.

Table 8. Mean annual and monthly total phosphorus (TP) loadings (t) for the baseline (1971–2000) as well as the projected changes (Δ,%) for scenarios ADC, ACU, AFD and ARP, the mean of the four scenarios, and the range of changes (ΔRange, t) for 2041−2070

Month	Baseline Observed (t)	ADC Future (t)	Δ ADC (%)	ACU Future (t)	Δ ACU (%)	AFD Future (t)	Δ AFD (%)	RP Future (t)	Δ ARP (%)	Mean ofΔ scenarios (t)	Range of Δs (ΔRange) (t)	Climate change signal If mean >Δ Range signal =strong
J	2.36	12.10	**413**	9.82	**317**	10.55	**347**	4.44	**88**	6.87	7.67	Weak
F	3.78	12.74	**237**	11.00	**191**	14.43	**282**	5.99	**59**	7.26	8.44	Weak
M	23.58	20.67	−12	25.38	8	22.25	−6	29.28	**24**	0.81	8.61	Weak
A	13.73	6.75	**−51**	51.58	**−62**	5.76	**−58**	10.47	**−24**	−6.7	5.31	Weak
M	1.68	1.70	**1**	13.33	−21	1.35	−20	1.55	−8	−0.20	0.37	Weak
J	0.92	0.53	−42	0.62	−33	0.55	−41	0.67	−28	−0.33	0.14	Weak
J	0.63	0.48	**−24**	0.53	−15	0.48	**−25**	0.64	1	−0.01	0.17	Weak
A	0.78	0.64	**−38**	0.55	**−29**	0.49	**−37**	0.55	**−29**	−0.22	0.15	Weak
S	0.82	0.89	9	0.87	**6**	0.84	**3**	1.25	**53**	0.14	0.41	Weak
O	2.07	2.43	**17**	1.76	−15	2.35	**13**	1.78	−14	0.01	0.67	Weak
N	2.72	2.65	−3	3.46	**27**	3.36	**24**	2.31	**−15**	0.28	1.15	Weak
D	2.74	4.96	**81**	5.71	**108**	4.57	**67**	4.06	**48**	2.08	1.65	Strong
Annual Mean	4.65	5.55	**19**	5.517	**19**	5.58	**20**	5.25	**13**	0.82	0.33	Strong
Annual Sum	55.83	66.54	**19**	66.20	**19**	66.98	**20**	63.00	**13**	9.86	3.98	Strong

The comparison of the mean to ΔRange is used to assess the strength of climate change signal of the ensemble mean. Bold values indicate statistically significant differences between the historical and future periods of study. Δ % are calculated following this equation: [(Future μ − Baseline μ)/Baseline μ] × 100, where μ is the 30-yr monthly average. ΔRange = ΔMax. − ΔMin.

Table 9. Mean annual and monthly total nitrogen (TN) loadings (t) for the baseline (1971–2000) as well as the projected changes (Δ, %) for scenarios ADC, ACU, AFD and ARP, the mean of the four scenarios, and the range of changes (ΔRange, t) for 2041–2070

Month	Baseline observed (t)	ADC future (t)	Δ ADC (%)	ACU future (t)	Δ ACU (%)	AFD future (t)	Δ AFD (%)	ARP future (t)	Δ ARP (%)	Mean of Δ scenarios (t)	Range of Δs (ΔRange) (t)	Climate change signal If mean >ΔRange signal =strong
J	26.46	**165.29**	**525**	**97.79**	**270**	**154.97**	**486**	**40.82**	**54**	88.26	124.47	Weak
F	31.84	**174.83**	**449**	**130.03**	**308**	**183.58**	**477**	**48.89**	**54**	102.50	134.70	Weak
M	300.75	**454.78**	**51**	**590.60**	**96**	**460.05**	**53**	**439.57**	**46**	185.50	151.03	Strong
A	436.50	**351.13**	**−20**	**323.02**	**−26**	**320.44**	**−27**	**502.81**	**15**	−62.15	182.37	Weak
M	119.43	136.40	14	109.90	−8	108.55	9	**131.04**	**10**	2.04	27.85	Weak
J	44.20	31.19	−29	**35.56**	**−20**	30.04	32	37.84	−14	−10.54	7.79	Weak
J	23.58	18.02	−24	21.94	−7	18.67	21	**24.79**	**5**	−2.72	6.77	Weak
A	36.62	**40.76**	**11**	36.19	−1	**31.44**	**14**	34.16	−7	−0.98	9.32	Weak
S	67.22	**87.82**	**31**	85.38	27	80.57	20	102.53	53	21.85	21.96	Weak
O	170.95	**251.87**	**48**	204.53	20	239.56	41	196.17	15	53.08	55.70	Weak
N	211.50	**296.02**	**40**	335.02	58	339.75	61	240.05	14	91.24	99.70	Weak
D	116.44	**265.17**	**128**	**235.80**	**103**	**271.83**	**133**	**158.54**	**36**	116.40	113.30	Strong
Annual Mean	132.04	**189.44**	**43**	**183.81**	**39**	**186.62**	**41**	**163.01**	**24**	48.71	26.34	Strong
Annual Sum	1584.44	**2273.28**	**43**	**2205.77**	**39**	**2239.47**	**41**	**1957.22**	**24**	584.50	282.25	Strong

The comparison of the mean to ΔRange is used to assess the strength of climate change signal of the ensemble mean. Bold values indicate statistically significant differences between the historical and future periods of study. Δ% is calculated following this equation: [(Future μ – Baseline μ)/Baseline μ] × 100, where μ is the 30-yr monthly average. ΔRange =ΔMax. – ΔMin.
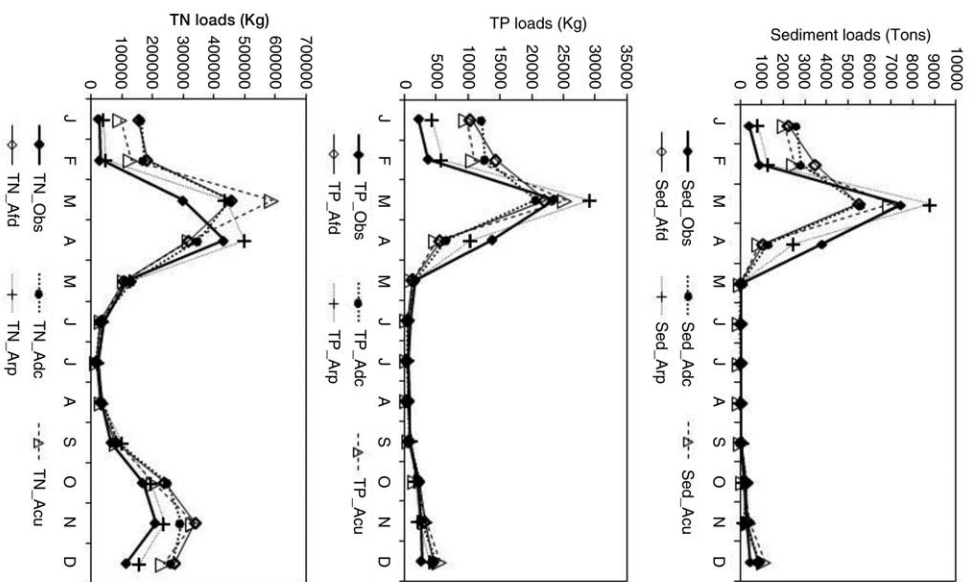

Fig. 8. Baseline (1971–2000) vs. future (2041–2070) simulated sediment (top), TP (middle) and TN (bottom) loads.

winter months of January and February, with loadings being three to five times greater than historical levels for the CGCM3 projections (175 to 494% for sediments, 191 to 413% for TP, 270 to 525% for TN) compared with 1.4 to 1.8 greater values for the Arpège projection (43 to 83% for sediments, 59 to 88% for TP, 54% for TN).

The increase in winter surface runoff and consequently soil erosion and nutrient transport can be explained by higher winter precipitation (16 to 33% for CGCM3 and 6% for Arpège) combined with higher temperatures (3.35 to 4.2°C for CGCM3 and 1.16°C for Arpège). This entails less snowfall and snow storage, but more rainfall and snowmelt and, consequently, more surface and total runoff, resulting in transport of a greater amount of sediments, TP, and TN from the land into water courses. These results suggest that the risk of erosion and nutrient loss are especially high in winter when fields are without soil protection in a "simulated business-as-usual" field operation management system. The differences in hydrology, sediment, and nutrient exports between the

projections of the CGCM3 model and the projection of Arpège model stem from the lower precipitation and temperatures projected by the latter model, which resulted in lower percentage changes in winter loads.

We believe that the high percentage changes (up to 400%) for runoff and nutrient loads during winter months (especially January) are caused by a concurrent increase in winter temperature and rainfall, resulting in spring flood occurring earlier in the year. A look at the sediment loadings (Table 7) shows that whilst baseline January loadings were only 437 t, the February, March, and April loadings were respectively 919, 7462, and 3819 t. The ADC projection, for example, projected sediment loadings of 2599, 2837, 5576, and 1342 t for January, February, March, and April, respectively. The differences between the baseline and ADC projection are therefore almost 2000, 1900, −1800, and −2500 t for January, February, March, and April, respectively. This represents an increase of about 3900 t almost equally distributed between January and February, and a decrease of similar magnitude (−4300 t) over March and April. This is in line with spring flood occurring earlier in the year. January and February percentage increases appear very high, probably because of the low baseline loadings. A look at absolute values, however, shows that future loads in January and February are often less than the peak baseline loads in March and April, which, overall, result in a net decrease of about 400 t. The annual increase is therefore not only due to the increase of the loads in January and February, due to the earlier spring flood, but also to warmer temperature and increase in precipitation through the months of September to December. Similar trends can be observed for TP loads and the other projections except ARP.

During the calibration and validation periods, SWAT showed a tendency to inaccurately simulate some intensive hydrological events and nutrient loads. It is therefore important to highlight that due to higher rainfall projections, results obtained within the Pike River watershed are conservative and climate change impact in the region could result in greater future erosion rates and nutrient losses than projected.

In spring, future runoff and nutrient loads tended to decrease, although projections were more uncertain, especially in March, when peak loading caused by spring snowmelt occurs. In fact, although March surface runoff was significantly decreased for the three CGCM3 projections ADC, ACU and AFA/AFD, the latter was the only projections resulting in a significant decrease in sediment loadings (26%). By contrast, the ARP projection projected significant increases in both runoff (15%) and sediment loading (18%). The TP peak load projections for March are even more uncertain as two projections (ADC, AFA-AFD) showed insignificant decreases in load, while the ACU and ARP projections projected insignificant (8%) and significant (24%) increases, respectively. The TN load peaked in April during the reference simulation but decreased significantly under all

three future CGCM3 projections. In contrast, the ARP projection projected increased TN loadings in April, but decreased surface runoff and sediment and TP loadings.

The decreases in the peak loadings are attributable to higher winter temperatures, which reduced snow storage and consequently spring snowmelt, runoff and nutrient transport. In fact, the two scenarios, AFD and ADC, which projected the higher increases in temperature and precipitation, also projected greater decreases in sediment (−26 and −25%, respectively) and TP (−6 and −12%, respectively) loads in March, and in TN loads in April (−27% for both simulations). The ARP projections projected a smaller increase in winter temperature, with a smaller impact on winter snow storage. The increases in runoff and nutrient loads projected in March for this projections stem from the very small changes in winter snowmelt (−2%) combined with increase in spring precipitation (15%). While all four projections projected a peak in surface runoff, sediment, and TP loadings in March, as in the reference scenario, all except the ARP projection projected an earlier TN peak, shifting from April to March.

It is difficult to explain why March TP loading from ACU projection tended to increase while sediment loadings and runoff tended to decrease. Deslandes et al. (2007) demonstrated that 70% of P in the Pike River Watershed was exported as particulate P. As TP is typically bound to sediments (Gollamudi et al. 2007) and sediment loads were projected to decrease in this watershed, a decrease in TP would also have been expected. However, some of the soils are highly saturated in P (Gangbazo et al. 2005) and received a large amount of fertilizer and manure (up to about 400 kg ha^{-1}) (Table 2). It is also known that a relatively significant amount of phosphorus can be transported through subsurface flow in the watershed with clayey soils, as a result of preferential flow (Gollamudi et al. 2007; Eastmann et al. 2010). SWAT does not model subsurface phosphorus processes, but a P concentration of 0.07 mg P L^{-1} was entered for the calibration parameter GWSOL_P (Table S2 – section GW.dbf) to account for the presence of P in subsurface flow. In doing so, subsurface P loads increase with subsurface flow. For the ACU projection there was a small decrease in surface runoff, but an increase in subsurface flow and streamflow was observed (Table S4), which could explain the small simulated increase in TP loads.

Subsurface flows in March were 178, 216, 175, and 120 mm for ADC, ACU, AFD, and ARP, respectively, compared with the baseline value of 102 mm. The slightly greater value with ACU increase may be due to lower February rainfall (a decrease of 3% compared with increases of 28, 56, and 4% for ADC, AFD, and ARP, respectively) followed by a wetter March (an increase of 35% for ACU vs. 26, 17, and 18% for ADC, AFD, and ARP, respectively). This may have allowed the soils to drain slightly more in February under the ACU, as compared with other projections. When March

precipitation occurred, the soils had therefore greater infiltration capacity under ACU than under the other projections. A greater soil infiltration capacity likely fostered subsurface flow at the expenses of surface flow. In contrast, the other projections had wetter soils in March due to a high amount of precipitation in February and March, which reduced the soil infiltration capacity and led to greater runoff and less subsurface flow. The reason why SWAT driven by the ACU projections projected a slight increase in March TP loadings while the other scenarios showed a decrease may therefore reside in antecedent low rainfall and soil moisture for the month of March, followed by wetter conditions.

It is noteworthy that processes of P infiltration in soils were not calibrated and are not simulated by SWAT. The concentration of 0.07 mg L^{-1} entered in SWAT subsurface flow to palliate this gap in the SWAT P routine represents an annual average concentration measured within the tiles of the watershed's agricultural sub-basins. In reality, the concentration would vary according to the timing of fertilizer applications, rainfall patterns, and soil moisture conditions (SWCS 2003). The GWSOLP concentration should therefore vary first during the year according to seasonal changes in hydrologic activity, and second with climate change (changes in rainfall pattern, intensity, and possible impacts in soil moisture condition). In the present modelling exercises, GWSOLP concentration is completely disconnected from climate as it is a constant value. The projected small increase in P might therefore be an artefact caused by the constant value of GWSOLP applied to all future simulations rather than a result from a real effect of climate change.

The simulations showed that NO_3 leaving the watershed contributed to about 30% of TN loads in January and February. During the rest of the year, subsurface NO_3 contributed between 55 and 100% of TN load. These numbers concur with results from Gollamudi et al. (2007), who studied N and P losses at field scale within the Pike River. Retention of NO_3 is generally minimal in soils because of its negative charge and this ion is therefore prone to leaching (Neitsch et al. 2011) and is found in subsurface flow. This probably explains why TN loadings did not perfectly mimic changes in surface runoff patterns, but were more closely related to total runoff.

The decrease projected in summer, in June, July, and August, could be explained by a decrease in precipitation and an increase in temperature, which resulted in increased evapotranspiration and decreased average runoff. It is important to note that even though the percentage changes in TP and TN seemed large, changes in absolute values were rather small, as loadings are generally small during summer. A 25% decrease in summer TP load (AFD in July), for example, corresponded to only a 156 kg TP (or 24 kg ha^{-1}) decrease in absolute terms.

SWAT was calibrated with load value rather than with instream nutrient concentrations. Therefore, the temporal accuracy of future loads depends on the relative proportion of changes in discharge and concentration. As explained earlier, the infiltration of nutrient in soils and subsurface processes are not well represented in SWAT, especially for phosphorus, and to palliate this gap a constant subsurface P concentration was set in the model and there was no way to accurately assess how this value could evolve in the future. As periods of low nutrient flow may have an important effect on nutrient loads, load simulations during future changes of relatively small hydrological alterations, such as those in March or in summer, will be less reliable than in periods associated with larger hydrological variations.

From these results, it is evident that the greatest impacts of climate change on streamflow and nutrient loads for the study area would occur during the winter and snowmelt periods, not only because the greatest changes in temperature, snowpack, and rainfall were projected for these periods, but also because the soils are more vulnerable to erosion and nutrient losses without plant cover.

Our results are consistent with those from previous hydrological studies performed using different bias-correction methods and hydrological models. Crossman et al. (2013), for instance, applied two IPCC SRES scenarios, A1b and A2, to a southern Ontario watershed, with statistically downscaled temperatures and precipitation using the CGCM3 climate model and the HBV-INCA-P hydrological and water quality model. Sulis et al. (2011) applied CRCM climate data with bias corrected with the delta method to the CATHY hydrological model to simulate snow accumulation and snowmelt processes in the des Anglais watershed in southern Québec. In contrast, Dayyani et al. (2012) used a CRCM projection without bias correction into the DRAIN-WARMF hydrological and water quality model and compared simulated outputs (1961–1990 vs. 2071–2100) for the intensively cultivated Saint-Esprit watershed in southern Québec. These three studies predicted that the increase in temperature and precipitation would probably shift the studied rivers towards a rain-fed, regime with less snow accumulation during the winter, but higher streamflow in January and February (up to +100%), and with spring flood moving from April to March. Strong decreases in summer flow (greater than −60%) were also projected by Sulis et al. (2011). Crossman et al. (2013) also predicted an increase in annual P streamflow concentration (+22.6 and +43.5%), while Dayyani et al. (2012) simulated significant increase in NO_3-N loadings for all seasons except spring.

Uncertainty Analysis

Uncertainties arise from the future geo-politico and social trends described by the different SRES GHGe scenarios but also from technical issues in modelling the physics of the climate. If the uncertainties in modelling the physics of the climate are too important, results of climate change impacts may not be discernible from

these uncertainties. In such instances, the mean of an ensemble of scenarios can provide a strong index to assess the overall outcomes of climate change impact (Gleckler et al. 2008). The degree of uncertainty (both due to GHGe projections and physical modelling) is determined by the range of the projection results. The larger the range of results; the greater the uncertainty (ΔRange in Tables 7, 8, and 9). If the changes given by the ensemble (the four scenarios) mean is greater than the range of the scenario results, the signal of climate change (mean of the scenarios) stands out from modelling uncertainties and is considered as robust (Boé et al. 2009). In the present study, the mean of the ensemble was often smaller than the full range of results given across the four projections (Tables 7, 8, and 9). Only the mean of December for sediment and TP loads, March and December for TN loads and the mean of annual projection for TP and TN loads were greater than the full range of results (ΔRange in Tables 7, 8, and 9) and could therefore be considered as robust.

These results are not unexpected since the scenarios were chosen to represent moderate changes (ADC, ACU), more extreme changes in winter (AFD), and smaller changes (ARP) in climate to cover a variety of results. The results showed that runoff, sediment, and nutrient loads were very sensitive to different climate projections. Inclusion of additional climate projections into the analyses might increase the mean of the ensemble and strengthen the overall impact of climate change projections.

Although the use of four projections is limited to adequately assess uncertainty, it provides an insight into various sources of climate change uncertainty, and their relative impacts on nutrient load projections. Several sources of uncertainty considered in this study include: (i) uncertainty stemming from initial conditions (given by ADC and ACU scenarios), (ii) uncertainty stemming from the choice of model version and domain (given by the comparison of ADC or ACU to AFD) and (iii) uncertainty stemming from the choice of model (given by the comparison of the three CGCM3 scenarios to ARP scenario). Table 10 shows the influence of each of these uncertainties on the range of results for TP loadings.

The differences in results stemming from a change in initial conditions is always much smaller than the mean of the four scenarios. This source of uncertainty contributes relatively little to the range of results and therefore the choice of initial conditions generally accounted for a small part of the total uncertainty. Even in February, when the difference in TP load changes between the two simulations (ADC and ACU) was 141%, the signal was much larger, with a mean increase in TP of 216%. Only projections for March and October appeared uncertain (or drawn into uncertainties) because the signal of climate change was smaller than the difference between the two scenarios.

Conclusions for the uncertainties emanating from a change in model version and domain are similar to uncertainties stemming from initial conditions. Differences between scenario AFD and the ADC or ACU scenarios remained relatively low compared with the signal of climate change, except for March and October. The differences between ADC or ACU and AFD were in most instances smaller than the difference between ADC and ACU, which used the same configuration of model but different initial conditions. This suggests that uncertainty emanating from the choice of model version and domain may in some cases be smaller than uncertainty stemming from initial conditions.

The uncertainty stemming from initial conditions is also called internal variability of the model and is considered as an irreducible error. In fact, changing initial conditions (starting days of the simulations) is like

Table 10. Assessment of the type/sources of uncertainty involved in the various climatic scenarios

Month	U initial conditions ADC vs. ACU	U model version AFD vs. ADC	U model version AFD vs. ACU	U model choice ARP vs. ADC	U model choice ARP vs. ACU	U model choice ARP vs. AFD	Range of Δs (%) ΔMax. − ΔMin	Mean of scenarios	Strength of signal vs. sources of uncertainty If mean >Umax signal = strong
J	97	66	31	325	228	259	325	291	Weak
F	46	45	91	178	133	223	223	192	Weak
M	20	7	13	37	17	30	37	3	Weak
A	12	7	4	27	39	34	39	−49	Weak
M	22	21	1	9	13	12	22	−12	Weak
J	10	2	8	15	5	13	15	−36	Weak
J	8	1	9	25	17	26	26	−16	Weak
A	12	20	8	11	1	9	20	−28	Weak
S	3	6	3	44	47	50	50	18	Weak
O	32	4	28	31	1	28	32	0	Weak
N	30	26	4	12	42	39	42	8	Weak
D	27	14	41	33	60	19	60	76	Strong
Average	**1**	**1**	**1**	**6**	**6**	**7**	**7**	**18**	**Strong**

All values are in percentage (%). U is uncertainty. U max is the maximum uncertainty. U = | Scenario1–Scenario2 |/Baseline. Range of Δ (in %) were calculated with the maximum and minimum Δs of Table 8 and average of all Δs of Table 8.

reproducing the chaotic nature of the climate or its natural variability (de Élia and Côté 2010; Frigon 2014).

The greatest difference in projections stems from uncertainty due to the choice of model. The ARP scenario introduced much smaller changes in precipitation and temperature and produced results that were considerably different from those of the CGCM3 scenarios. On the one hand, the addition of this scenario allows for incorporating more sources of uncertainty and more possibilities of climate change results and, consequently, results in the production of a more comprehensive picture of results for future planning. On the other hand, it considerably enlarges the level of uncertainty for modelling results. In this study, the climate change signal for TP was imprecise and uncertain for all months of the year except December. However, the analysis showed that different directions of change are possible and need to be planned for.

The overall increase in mean annual TP is nonetheless much certain (mean change of 18% (10 t P yr^{-1}) vs. range of uncertainty of 7% (4 t P yr^{-1})).

Implications for Water Quality in the Misissquoi Bay

Whereas the set criteria stipulate that TP delivery should not exceed 38.9 t yr^{-1} (for the Québec portion of Rock, Missisquoi, and Pike watersheds) (Beck et al. 2012), SWAT estimated P load for the Pike River watershed alone for the historical period (1971–2000) at 55 t P yr^{-1}, increasing to 65 ± 4 t yr^{-1} in the future (2041–2070). Although seasonal changes were less certain than annual changes, seasonal, and monthly projections showed that erosion events and nutrient transport would begin earlier in the winter/spring period. Best management practices to protect soils must therefore be implemented to account for this possibility.

The Missisquoi Bay water quality criteria of 0.03 mg P L^{-1} translates into a P loading capacity of 97.2 t yr^{-1} for the entire bay. Results from this study suggest that targets for the Missisquoi Bay water quality may have to be reviewed given the new projected hydrological and nutrient delivery regimes. In fact, with a significant annual TP addition of 10.0 t yr^{-1} TP (18%), a significant annual TN addition of 571 t TN yr^{-1} (40%) and respective streamflow increases of 20%, it appears that the nutrient concentration into the bay is likely to increase in the future. Potential increases in nutrient loading from the other watersheds draining into the bay (Missisquoi and Rock River watersheds), which present similar characteristics to the Pike River watershed, might exacerbate the NPS pollution in the Missisquoi Bay in a future changing climate.

CONCLUSION

In order to assess the impacts of climate change on the Missisquoi Bay water quality, a modified version of SWAT 2005 model (SWAT$_{qc}$), adapted to Québec agroclimatic conditions coupled with future climate projections was used to simulate sediment and nutrient exports into the Missisquoi Bay. Potential changes in the Pike River watershed water yields, and TN and TP loadings were assessed for the 2041–2070 horizon based on the 1971–2000 reference period.

Simulated mean annual streamflow increased by 11% (4.71 mm) to 20% (8.77 mm). Increases in mean annual sediment, TP and TN loadings ranged from 1 to 7%, from 13 to 20%, and from 24 to 43%, respectively. This study demonstrates that different sources of climate change uncertainty have different impacts on projected nutrient loads; the greatest uncertainty stemmed from the choice of climate model. The study could be improved by incorporating more scenarios into the analyses. The average (across all scenarios) increase in scenario annual runoff, sediment and nutrient loads were consistently higher than the full range of results (uncertainty). Results from SWAT modelling using the four ensemble members and the IPCC A2 scenario suggest that yearly runoff, sediment, TP, and TN loads will increase by about 13 mm, 409 t, 10 t, and 585 t, respectively. Higher temperatures, rainfall, and earlier snowmelt, were generally predicted for the winter season. Furthermore, future winter streamflow and nutrient loadings were projected to increase fivefold compared with historic levels for the three CGCM3 scenarios, while the scenario simulated with the Arpège model projected smaller increases 1.5- to 2-fold greater than the historic levels. Peak discharges in TN loads were projected to shift from April to March. Future summer and spring streamflow and sediment and nutrient loadings were projected to decreases to a smaller extent than the increases simulated for winter and fall.

If the projected increases in nutrient loadings happen in the future, this will certainly make it more difficult to achieve the Missisquoi Bay water quality standards of 0.03 mg P L^{-1} set to prevent eutrophication and the incidence of cyanobacterial blooms within Lake Champlain.

Arheimer, B., Andreasson, J., Fogelberg, S., Johnsson, H., Pers, C. B. and Persson, K. 2005. Climate change impact on water quality: Model results from southern Sweden. Ambio **34**: 559–566.

Arnold, J. G., Srinivasan, R., Muttiah, R. S. and Williams, J. R. 1998. Large area hydrologic modelling and assessment part I: Model development. J. Am. Water Resour. Assoc. **34**: 73–89.

Beck, E., van Bochove, E., Schmetzler, E. and Leblanc, D. 2012. Missisquoi Bay critical source study. International Missisquoi Bay Study Board. Final report to the International Joint Comission.

Blais, S. 2002. La problématique des cyanobactéties (algues bleu–vert) à la baie Mississquoi en 2001. Agrosolutions **13**: 103–110.

Boé, J., Terray, L., Martin, E. and Habets, F. 2009. Projected changes in components of the hydrological cycle in French river basins during the 21st century. Water Resour. Res. **45**: W08426.

Booty, W., Lam, D., Bowen, G., Resler, O. and Leon, L. 2005. Modelling changes in stream water quality due to climate change in a southern Ontario watershed. Can. Water Resour. J. **30**: 211–226.

Borah, D. K. and Bera, M. 2003. Watershed-scale hydrologic and nonpoint-source pollution models: Review of mathematical bases. Trans. ASAE **46**: 1553–1566.

Borah, D. K., Xia, R. and Bera, M. 2002. DWSM – A dynamic watershed simulation model. *In* V. P. Singh and D. K. Frevert, eds. Mathematical models of small watershed hydrology and applications. Water Res Publ., Highlands Ranch, CO.

Bouraoui, F., Galbiati, L. and Bidoglio, G. 2002. Climate change impacts on nutrient loads in the Yorkshire Ouse catchment (UK). Hydrol. Earth Syst. Sci. **6**: 197–209.

Boyer, C., Chaumont, D., Chartier, I. and Roy, A. G. 2010. Impact of climate change on the hydrology of St. Lawrence tributaries. J. Hydrol. **384**: 65–83.

Caya, D. and Laprise, R. 1999. A semi-implicit semi-lagrangian regional climate model: The Canadian RCM. Mon. Weather Rev. **127**: 341–362.

Crossman, J., Futter, M. N., Oni, S. K., Whitehead, P. G., Jin, L., Butterfield, D., Baulch, H. M. and Dillon, P. J. 2013. Impacts of climate change on hydrology and water quality: Future proofing management strategies in the Lake Simcoe watershed, Canada. J. Great Lakes Res. **39**: 19–32.

Dayyani, S., Prasher, S. O., Madani, A. and Madramootoo, C. A. 2012. Impact of climate change on the hydrology and nitrogen pollution in a tile drained agricultural watershed in eastern Canada. Trans. ASABE **55**: 389–401.

de Elia, R. and Cote, H. 2009. Climate and climate change sensitivity to model configuration in the Canadian RCM over North America. Meteorol. Z. **19**: 325–339.

Deslandes, J., Michaud, A. R. and Bonn, F. 2004. Use of GIS and remote sensing to develop indicators of phosphorus nonpoint source pollution in the Pike River basin. Pages 271–290 *in* T. O. Manley, P. L. Manley, and T. B. Mihuc, eds. Lake Champlain: partnerships and research in the new millennium. Kluwer Academic/Plenum Publ., New York, NY.

Deslandes, J., Beaudin, I., Michaud, A., Bonn, F. and Madramootoo, C. A. 2007. Influence of landscape and cropping system on phosphorus mobility within the Pike River watershed of Southwestern Quebec: Model parameterization and validation. Can. Water Resour. J. **32**: 21–42.

Douville, H., Chauvin, F., Planton, S., Royer, J.-F., Salas-Mélia, D. and Tyteca, S. 2002. Sensitivity of the hydrological cycle to increasing amounts of greenhouse gases and aerosols. Clim. Dynam. **20**: 45–68.

Eastman, M., Gollamudi, A., Stämpfli, N., Madramootoo, C. A. and Sarangi, A. 2010. Comparative evaluation of phosphorus losses from subsurface and naturally drained agricultural fieds in the Pike River watershed of Québec, Canada. Agric. Water Manage. **97**: 596–604.

Engel, B., Storm, D., White, M., Arnold, J. and Arabi, M. 2007. A hydrologic/water quality model application protocol. J. Am. Water Resour. Assoc. **43**: 1223–1236.

Environment Canada. 2007. Canadian climate data on-line. Customized Search. [Online] Available: http://www.climate. weatheroffice.gc.ca/climateData/canada_e.html [2008 July].

Fortin, N., Rocio, A. R., Jing, H., Pick, F., Bird, D. and Greer, C. W. 2010. Detection of microcystin-producing cyanobacteria in Missisquoi Bay, Québec, Canada, using quantitative PCR. Appl. Environ. Microbiol. **76**: 5105–5112.

Fowler, H. J., Blenkinsop, S. and Tebaldi, C. 2007. Linking climate change modelling to impacts studies: Recent advances in downscaling techniques for hydrological modelling. Int. J. Climatol. **27**: 1547–1578.

Frigon, A., Biljana, M. and Slivitzki, M. 2010. Sensitivity of runoff and projected changes in runoff over Quebec to the update interval of lateral boundary conditions in the Canadian RCM. Meteor. Z. **19**: 225–236.

Gagnon, P., Konan, B., Rousseau, A. N. and Slivitzky, M. 2009. Hydrometeorological validation of a Canadian regional climate model simulation within the Chaudière and Châteauguay watersheds (Québec, Canada). Can. J. Civ. Eng. **36**: 253–266.

Gangbazo, G., Roy, J. and Le Page, A. 2005. Capacité de support des activités agricoles par les rivières: le cas du Phosphore Total. MDEP. Québec. [Online] Available: http://www.mddep.gouv.qc.ca/eau/bassinversant/capacite-phosphore.pdf [2014 May].

Gibelin, A.-L. and Déqué, M. 2003. Anthropogenic climate change over the Mediterranean region simulated by a global variable resolution model. Clim. Dyn. **20**: 327–339.

Gleckler, P. J., Taylor, K. E. and Doutriaux, C. 2008. Performance metrics for climate models. J. Geophys. Res. **13**: D06104.

Gollamudi, A., Madramootoo, C. A. and Enright, P. 2007. Water quality modelling of two agricultural fields in southern Quebec using SWAT. Trans. ASABE **50**: 1973–1980.

Gombault, C., Sottile, M-F., Ngwa, F. F., Madramootoo, C. A., Michaud, A. R., Beaudin, I. and Chikhaoui, M. 2015. Modelling climate change impacts on the hydology of an agricultural watershed in southern Québec. Can. Water Resour. J. **40**: 71–86. doi: 10.1080/07011784.2014.985509.

Hargreaves, G. L., Hargreaves, G. H. and Riley, J. P. 1985. Agricultural benefits for Senegal River Basin. J. Irrig. Drain E-ASCE **11**: 113–124.

Hegman, W., Wang, D. and Borer, C. 1999. Estimation of Lake Champlain Basin wide nonpoint source phosphorus export. Lake Champlain Basin Program: Technical Report No. 31. Grand Isle, VT. 99 pp.

Intergovernmental Panel on Climate Change. 2007. Climate change 2007: The physical science basis. Contribution of Working Group I to the Fourth Assessment Report of the Intergovernmental Panel on Climate Change. S. Solomon, D. Qin, M. Manning, Z. Chen, M. Marquis, K. B. Averyt, M. Tignor, and H. L. Miller, eds. Cambridge University Press, Cambridge, UK. 996 pp.

Jha, M., Arnold, J. G., Gassman, P. W., Giorgi, F. and Gu, R. R. 2006. Climate change sensitivity assessment on upper Mississippi River Basin Streamflows using SWAT. J. Am. Water Res. Assoc. **42**: 997–1015. doi: 10.1111/j.1752-1688. 2006.tb04510.x.

Jha, M., Pan, Z., Tackle, E. S. and Gu, R. 2004. Impacts of climate change on stream flow in the Upper Mississippi River

Basin: A regional climate model perspective. J. Geophys. Res. Atmos. D09105.

Jamieson, A., Madramootoo, C. A. and Enright, P. 2003. Phosphorus losses in surface and subsurface runoff from a snowmelt event on an agricultural field in Quebec. Can. Biosyst. Eng. **45**: 1–17.

Jeppesen, E., Kronvang, B., Meerhoff, M., Søndergaard, M., Hansen, K. M., Andersen, H. E., Lauridsen, T. L., Liboriussen, L., Beklioglu, M., Ozen, A. and Olesen, J. E. 2009. Climate change effects on runoff, catchment phosphorus loading and lake ecological state, and potential adaptations. J. Environ. Qual. **38**: 1930–1941.

La Financière agricole. 2008. Événements – État des cultures. Gouvernement du Québec. [Online] Available: http://www.fadq.qc.ca/acces_medias/evenements/etats_des_cultures/etat_des_cultures_2012.html. [2008 Sep. and 2011 Jul.].

Lake Champlain Basin Program. 2012. State of of the lake and ecosystem indicators report – 2012. [Online] Available: http://sol.lcbp.org/phosphorus_where-does-p-come-from.html [2013 December].

Lettenmaier, D., Major, D., Poff, L. and Running, S. 2008. Water resources. The effects of climate change on agriculture, land resources, water resources, and biodiversity in the United States. A report by the U.S. Climate Change Science Program and the Subcommittee on Global Change Research, Washington, DC. 362 pp.

McFarlane, N. A., Scinocca, J. F., Lazare, M., Harvey, R., Verseghy, D. and Li, J. 2005. The CCCma third generation atmospheric general circulation model. Rapport interne du Centre Canadien de la Modélisation et de l'Analyse Climatique, 25p. [Online] Available: http://www.cccma.ec.gc.ca/papers/jscinocca/AGCM3_report.pdf [2013 Dec.].

Michaud, A. R., Beaudin, I., Deslandes, J., Bonn, F. and Madramootoo, C. A. 2007. SWAT-predicted influence of different landscape and cropping system alterations on phosphorus mobility within the Pike River watershed of south-western Québec. Can. J. Soil. Sci. **87**: 329–344.

Michaud, A., Deslandes, J. and Desjardin, J. 2004a. Réseau d'actions concertées en bassins versants agricoles. [Network of holistic undertakings on agricultural watersheds] Rapport Final Projet 212, to the Fonds d'action québécois pour le développement durable. Institut de Recherche et Developpment durable en Agroenvironnement. Québec City, QC. 23 pp.

Michaud, A. R., Lauzier, R. and Laverdière, M. R. 2002. Description du système de transfert du phosphore dans le bassin-versant du ruisseau au Castor. Agrosol **13**: 124–139.

Michaud, A. R., Lauzier, R. and Laverdière, M. R. 2004b. Temporal and spatial variability in non-point source phosphorus in relation to agricultural production and terrestrial indicators. Pages 97–121 *in* T. O. Manley, P. L. Manley, and T. B. Mihuc, eds. Lake Champlain: Partnerships and research in the new millennium. Kluwer Academic/Plenum Publ., New York, NY.

Michaud, A., Seydoux, S., Beaudin, I. and Gombault, C. 2008. Beneficial management practices and water quality: Hydrological modelling of two basins in the Montérégie Region (Québec). National Agri-Environmental Standards Initiative Technical Series Report No. 4-65. Québec. 129 pp.

Ministère du Développement durable, de l'Environnement et des Parcs. 2007. Compiled by the Ministry of Sustainable Development, Environment and Parks from: Statistics Canada, Census of Agriculture 2006. [Online] Available: http://www.statcan.ca/francais/freepub/95-629-XIF/2007000/tables_menu_f.htm [2007 Dec. 21] and Census of Agriculture 2001, farm and farm operator data. CD-ROM # 95F0304XCB [2008 July].

Ministère du Développement durable, de l'Environnement et des Parcs. 2008. Suivi Hydrologique de stations hydrométriques. Centre D'Expertise Hydrométrique du Québec. [Online] Available: http://www.cehq.gouv.qc.ca/suivihydro/default.asp [2008 July].

Ministère du Développement durable, de l'Environnement et des Parcs. 2012. Portrait de la qualité des eaux de surface au Québec 1999–2008. Direction du suivi de l'état de l'environnement. Québec. 97 pp.

Moriasi, D. N., Arnold, J. G., Van Liew, M. W., Bingner, R. L., Harmel, R. D. and Veith, T. L. 2007. Model evaluation guidelines for systematic quantification of accuracy in watershed simulations. Trans. ASABE. **50**: 885–900.

Music, B. 2011. CRCM: a promising tool for studying the hydrological cycle in a changing climate. [Online] Available at: http://www.ouranos.ca/en/newsletter/documents/newsletter-BM2011En_002.pdf [2014 May].

Nakicenovic, N., Alcamo, J., Davis, G., de Vries, B., Fenhann, J., Gaffin, S., Gregory, K., Grübler, A., Jung, T. Y., Kram, T., Rovere, E. L. L., Michaelis, L., Mori, S., Morita, T., Pepper, W., Pitcher, H., Price, L., Riahi, K., Roehrl, A., Rogner, H. H., Sankovski, A., Schlesinger, M., Shukla, P., Smith, S., Swart, R., van Rooijen, H., Victor, N. and Dadi, Z. 2000. IPCC special report on emissions scenarios. Cambridge University Press, Cambridge, UK.

NARCCAP. 2007. North American Regional Climate Change Assessment Program. [Online] Available: http://www.narccap.ucar.edu/about/index.html [2014 May].

Neitsch, S. L., Arnold, J. G., Kiniry, J. R. and Williams, J. R. 2011. Soil and water assessment tool theoretical documentation version 2009. Texas Water Resources Institute, College Station, TX. 647 pp.

Ouranos. 2010. Savoir s'adapter aux changements climatiques. C. DesJarlais, M. Allard, D. Bélanger, A. Blondlot, A. Bouffard, A. Bourque, D. Chaumont, P. Gosselin, D. Houle, C. Larrivée, N. Lease, A. T. Pham, R. Roy, J.-P. Savard, R. Turcotte, and C. Villeneuve, eds. Montréal, QC. 128 pp. [Online] Avalaible http://www.ouranos.ca/fr/pdf/53_sscc_21_06_lr.pdf [2011 Nov.].

Overton, D. E. 1966. Muskingum flood routing of upland stream flow. J. Hydrol. **4**: 185–200.

Pierson, D., Arvola, L., Allott, N., Järvinen, M., Jennings, E., May, L., Moore, K. and Schneiderman, E. 2010. Modelling the effects of climate change on the supply of phosphate-phosphorus. Chapter 9 *in* G. George, ed. The impact of climate change on European lakes. Aquatic Ecologic Series. 2010. Vol. 4. Springer Science, New York, NY.

Plummer, D. A., Caya, D., Frigon, A., Côté, H., Giguère, M., Paquin, D., Biner, S., Harvey, R. and de Elia, R. 2006. Climate and climate change over North America as simulated by the Canadian RCM. J. Clim. **19**: 3112–3132.

Rahman, M., Bolisetti, T. and Balachandar, R. 2010. Effect of climate change on low-flow conditions in the Ruscom River watershed, Ontario. Trans. ASABE **53**: 1521–1532.

Scinocca, J. F. and McFarlane, N. A. 2004. The variability of modelled tropical precipitation. J. Atmos. Sci. **61**: 1993–2015.

Sharpley, A. N., Daniel, T., Sims, T., Lemuyon, J., Stevens, R. and Parry, R. 2003. Agricultural phosphorus and eutrophication. 2nd ed. US Department of Agriculture–Agricultural Research Service, Washington, DC. ARS-149 eds. 44 pp.

Soil and Water Conservation Society. 2003. Conservation implications of climate change: Soil erosion and runoff from cropland. Iowa. Report No 68-4A75-2-98. 25 pp.

Sulis, M., **Paniconi, C.**, **Rivard, C.**, **Harvey, R. and Chaumont, D. 2011.** Assessment of climate change impacts at the catchment scale with a detailed hydrological model of surface–subsurface interactions and comparison with a land surface model. Water Resour. Res. **47**.

Union Québécqoise pour la Conservation de la Nature. 2005. La gestion du territoire et des activités agricoles dans le cadre de l'approche par bassin versant. Rapport présenté en mars 2005 au Ministère de l'Environnement du Québec, QC.

US Departement of Agriculture–Soil Conservation Service 1972. Section 4. Hydrology. *In* National Engineering Handbook. USDA–SCS, Washinghton, DC.

Walker, W. 1998. Flux, stream loads computations. Version 5.0. Environmental Laboratory, US Army Engineers, Waterways Experiment Station, Vicksburg, MS.

Williams, J. R. 1975. Sediment routing for agricultural watersheds. J. Am. Water Resour. Assoc. **11**: 965–974.

Williams, J. R. and Hann, R. W. 1978. Optimal operation of large agricultural watersheds with water quality constraints. Technical Report No. 96. Texas Water Resources Institute, Texas A&M University, College Station, TX.